

See discussions, stats, and author profiles for this publication at: <https://www.researchgate.net/publication/272135887>

# Protonation Pattern, Tautomerism, Conformerism, and Physicochemical Analysis in New Crystal Forms of the Antibiotic Doxycycline

ARTICLE in CRYSTAL GROWTH & DESIGN · AUGUST 2014

Impact Factor: 4.89 · DOI: 10.1021/cg500877z

---

READS

14

## 9 AUTHORS, INCLUDING:



Olimpia Santos

Universidade Federal de Alfenas

9 PUBLICATIONS 11 CITATIONS

[SEE PROFILE](#)



Alexandre Legendre

São Paulo State University

24 PUBLICATIONS 126 CITATIONS

[SEE PROFILE](#)



I. M. R. Landre

Universidade Federal de Alfenas

15 PUBLICATIONS 30 CITATIONS

[SEE PROFILE](#)



Antonio Carlos Doriguetto

Universidade Federal de Alfenas

119 PUBLICATIONS 888 CITATIONS

[SEE PROFILE](#)

# Protonation Pattern, Tautomerism, Conformerism, and Physicochemical Analysis in New Crystal Forms of the Antibiotic Doxycycline

Olímpia M. M. Santos,<sup>†,‡</sup> Douglas M. Silva,<sup>†</sup> Felipe T. Martins,<sup>\*,‡</sup> Alexandre O. Legendre,<sup>†,§</sup> Lilian C. Azarias,<sup>†</sup> Iara M. L. Rosa,<sup>†</sup> Person P. Neves,<sup>||</sup> Magali B. de Araujo,<sup>†</sup> and Antonio C. Doriguetto<sup>\*,†</sup>

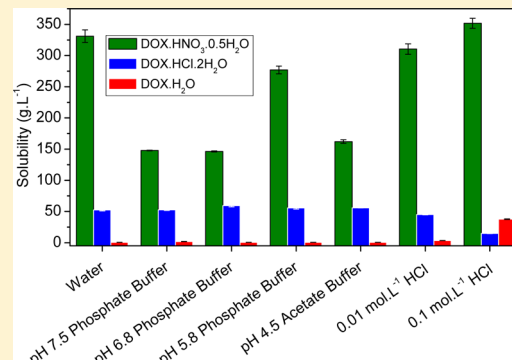
<sup>†</sup>Instituto de Química, <sup>||</sup>Instituto de Ciências Exatas, and <sup>‡</sup>Faculdade de Ciências Farmacêuticas, UNIFAL-MG - Universidade Federal de Alfenas, Campus Sede, Rua Gabriel Monteiro da Silva no 700, CEP 37130-000, Alfenas, Minas Gerais, Brazil

<sup>‡</sup>Instituto de Química, Universidade Federal de Goiás, Campus Samambaia, CP 131, CEP 74001-970, Goiânia, Goiás, Brazil

<sup>§</sup>Faculdade de Ciências, UNESP - Univ Estadual Paulista, Campus Bauru, Departamento de Química, Av. Eng. Luiz Edmundo Carrijo Coube no 14-01, CEP 17033-360, Bauru, São Paulo, Brazil

## S Supporting Information

**ABSTRACT:** Doxycycline (DOX) is a tetracycline class drug that is used worldwide as a broad-spectrum antibiotic. Although its clinical importance and use have been known since the 1960s, only four crystal forms have been reported until now. These are doxycycline hydrate (DOX.HYC), which is a hydrochloride salt hemiehanolate-hemihydrate; its isomorphous hydrobromide, hydrochloride salt dihydrate (DOX·HCl·2H<sub>2</sub>O); and doxycycline monohydrate (DOX·H<sub>2</sub>O). Here we report the preparation of two new multicomponent molecular crystal forms of doxycycline and their crystal structure determination along with their melting temperature, aqueous solubility, and time-dependent dissolution profile. These crystal forms are a hydronitrate salt hemihydrate (DOX·HNO<sub>3</sub>·0.5H<sub>2</sub>O) and an acetic acid solvate dihydrate (DOX·HAc·2H<sub>2</sub>O). The two new doxycycline crystal forms were compared with known forms, including DOX·HCl·2H<sub>2</sub>O, the structure of which was redetermined in this work. The structural variability of the protonation patterns, tautomerism of the keto-enolate moieties, and conformation of the amide groups was observed for these compounds. While intramolecular rings assembled through resonance-assisted hydrogen bond (RAHB) were observed in both fused keto-enol moieties of all structures, DOX·HCl·2H<sub>2</sub>O and DOX·HNO<sub>3</sub>·0.5H<sub>2</sub>O have another RAHB encompassing the protonated amide carbonyl oxygen and the enolate oxygen. These two crystal forms have a net positive charge on their drug molecule as DOX·HYC. They crystallize with the *N,N*-dimethylamine and amide carbonyl groups protonated and the neighboring hydroxyl group deprotonated. DOX, by contrast, crystallizes as a zwitterion in DOX·HAc·2H<sub>2</sub>O similarly to DOX·H<sub>2</sub>O. Their amide carbonyl oxygens are not protonated, which differs from the salt forms. DOX·HNO<sub>3</sub>·0.5H<sub>2</sub>O presents as two tautomers that are similar to those of DOX·HYC, namely, T1, in which the enolate oxygen is next to the protonated amine group, and T2, with the carbonyl oxygen close to the protonated amine group. These tautomers also differ in their amide conformations due to a rotation of ca. 180° on the C-C bond axis of the amide group, which directs the protonated carbonyl oxygen toward the enolate oxygen. DOX·HCl·2H<sub>2</sub>O has only one T1-like tautomer and therefore only one amide conformation similar to that of T1. A T1-like keto-enolate tautomer is present in DOX·HAc·2H<sub>2</sub>O, which exhibits an amide conformation similar to that of T2. Thermal (DSC and TG) and infrared analysis and equilibrium solubility, dissolution profiles, and forced degradation studies were performed to both new and known DOX forms. The results were correlated with their structural features. DOX·HNO<sub>3</sub>·0.5H<sub>2</sub>O was the most soluble form. This new form was also more stable than the commercial DOX·HYC in the oxidation test and more stable than commercial DOX·H<sub>2</sub>O against acid and basic hydrolysis and in the photostability study. DOX·HNO<sub>3</sub>·0.5H<sub>2</sub>O and DOX·HYC (commercial form) were observed to have similar drug release behaviors from capsules ( $F_2 > 50$ ) and therefore they could be interchangeable.



## 1. INTRODUCTION

Doxycycline ( $\alpha$ -6-deoxyoxytetracycline, DOX – Figure 1) is an active tetracycline class pharmaceutical agent (API) that is used worldwide as a broad-spectrum antibiotic due to its strong and powerful effect against several microorganisms groups, including *Legionella*, *Chlamydia*, *Mycoplasma*, and *Borrelia rickettsiae*.<sup>1,2</sup> DOX is one of the most important tetracycline

drugs currently in clinical use and is mainly employed in treating respiratory and urinary tract infections and as part of atypical pneumonia therapy.<sup>1–3</sup> This API combines high

**Received:** November 30, 2013

**Revised:** July 3, 2014

**Published:** July 10, 2014

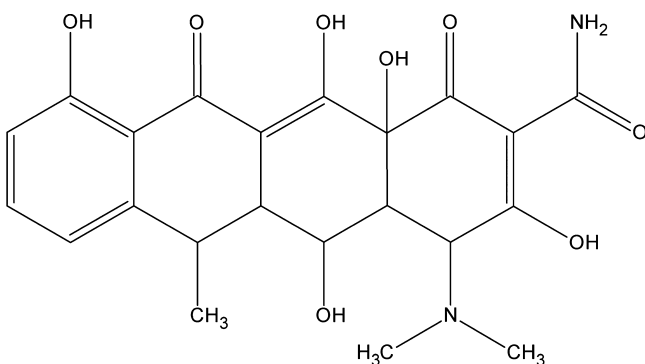


Figure 1. Chemical diagram of doxycycline (DOX).

efficacy, slow clearance (and therefore practical single-dosage schemes), low incidence of side effects, and low cost of treatment.<sup>4</sup> Even though the use of tetracycline drugs has decreased in the past two decades due to the emergence of new classes of antibiotics,<sup>5</sup> the therapeutic relevance of DOX has been retained due to recent discoveries of new applications for the treatment of Anthrax, Lyme disease, Plague, *P. falciparum* (malaria), and community-acquired methicillin-resistant *Staphylococcus aureus*.<sup>6</sup>

Even though its clinical importance and use have been known since the 1960s, only four crystal forms of DOX have been reported until now. Doxycycline hydrate (DOX-HYC) is a doxycycline hemiethanolate-hemihydrate hydrochloride that crystallizes with two distinct doxycycline tautomers in the asymmetric unit whose isomorphous hydrobromide was determined in the 1970s.<sup>7</sup> More recently, the crystal structures of doxycycline monohydrate (DOX·H<sub>2</sub>O), which crystallizes with only one zwitterionic molecule in the lattice,<sup>8</sup> and doxycycline hydrochloride salt dihydrate (DOX·HCl·2H<sub>2</sub>O)<sup>9</sup> were reported. Both DOX-HYC and DOX·H<sub>2</sub>O are incorporated into solid dosage forms under brand names such as DORYX, PERIOSTAT, ATRIDOX, and VIBRAMYCIN (DOX-HYC) or MONODOX and ORACEA (DOX·H<sub>2</sub>O). The crystal structure of the anhydrous hydrochloride salt 6-epimer ( $\beta$ -6-deoxyoxotetracycline) of the doxycycline is also known.<sup>10</sup>

It is well-known that crystal forms of the same API can have different solid state properties, composition, and structural variability.<sup>11</sup> The following has been reported for DOX: DOX·H<sub>2</sub>O has slower dissolution kinetics and lower equilibrium solubility than DOX-HYC, which could be due primarily to the hindered hydration of DOX·H<sub>2</sub>O due to the saturation of hydrogen-bonding (HB) functionalities in the lattice.<sup>8</sup> In addition, inspection of the DOX-HYC and DOX·H<sub>2</sub>O crystal structures has revealed interesting intramolecular differences in terms of protonation pattern, tautomerism of the keto–enolate moiety, and conformation of the amide group.<sup>7,8</sup> Such structural features lead to the formation of a further resonance-assisted hydrogen bond (RAHB) encompassing the enolate and amide atoms because the two fused keto–enol moieties are also stabilized by the RAHB. The resonance-assistance effects of HB are based on planarity descriptors and bond lengths; these are better explored in this study for both known crystal forms of DOX. The crystal structure analyses for three solid state phases of DOX, two of which were performed for the first time, are reported. These structures consist of a hydrochloride salt dihydrate (DOX·HCl·2H<sub>2</sub>O),<sup>9</sup> a nitrate salt hemihydrate (DOX·HNO<sub>3</sub>·0.5H<sub>2</sub>O), and an acetic acid solvate

dihydrate (DOX·HAc·2H<sub>2</sub>O). It is important to emphasize that the DOX·HCl·2H<sub>2</sub>O crystal structure remained unknown until March 2013 when the structure was reported by Heinemann et al. (2013).<sup>9</sup> These authors have also highlighted that, since the discovery of tetracyclines, much work has been devoted to determining the protonation–deprotonation equilibria, the tautomerism, and the geometry adopted depending on protonation and environmental states without satisfactory answers.<sup>9</sup>

The two new structures reported here and the three previously reported structures are all compared in terms of their intra (protonation pattern, tautomerism, and conformerism) and intermolecular features. Thermal behavior, water solubility, and dissolution rate of the DOX·HNO<sub>3</sub>·0.5H<sub>2</sub>O and DOX·HAc·2H<sub>2</sub>O forms could be determined and correlated to either salt or solvate nature. Their pharmaceutical performances were similarly demonstrated to be equivalent to that of DOX-HYC, which is marketed as having high water solubility.

## 2. EXPERIMENTAL SECTION

**2.1. Crystal Preparation.** Crystals of DOX·H<sub>2</sub>O were prepared according to a procedure described in the relevant literature.<sup>8</sup> Briefly, an amount of DOX-HYC (5 g) was dissolved in distilled water (200 mL) and neutralized by dropwise addition of a 1 mol L<sup>-1</sup> sodium hydroxide aqueous solution. The authenticity and purity of DOX·H<sub>2</sub>O were first checked by powder X-ray diffraction before the compound was used to prepare the crystal modifications. To prepare the new crystal forms described in this study, a quantity of DOX·H<sub>2</sub>O was added to 6 mol L<sup>-1</sup> aqueous solutions of either hydrochloric acid (DOX·HCl·2H<sub>2</sub>O) or nitric acid (DOX·HNO<sub>3</sub>·0.5H<sub>2</sub>O) at room temperature until a surplus of undissolved solid material (saturation) was observed. In the case of DOX·HAc·2H<sub>2</sub>O, a saturated solution of DOX·H<sub>2</sub>O was prepared under magnetic stirring in a 1:1 (v:v) glacial acetic acid/water mixture as described for the hydrochloride and nitrate salt hydrates. Next, the suspensions were filtered through a 0.45  $\mu$ m filter (Millipore) and the filtrates were left to stand in the dark for 4 days.

Well-shaped and suitably sized single crystals of DOX·HCl·2H<sub>2</sub>O, DOX·HNO<sub>3</sub>·0.5H<sub>2</sub>O, and DOX·HAc·2H<sub>2</sub>O were selected for the single crystal X-ray diffraction analysis. The remaining crystals, including those obtained for DOX·H<sub>2</sub>O and DOX-HYC, were sieved using a stainless steel mesh. The size fraction between 106  $\mu$ m (150 mesh) and 75  $\mu$ m (200 mesh) was selected for further studies.

**2.2. Single-Crystal X-ray Diffraction Structure Determination Experiment.** The single-crystal X-ray diffraction measurements for DOX·HCl·2H<sub>2</sub>O, DOX·HNO<sub>3</sub>·0.5H<sub>2</sub>O, and DOX·HAc·2H<sub>2</sub>O were performed at room temperature on a Gemini A-Ultra diffractometer equipped with an Atlas CCD detector using graphite-monochromatized Mo or Cu K $\alpha$  beams. The programs CrysAlis CCD and CrysAlis RED<sup>12</sup> were used for data collection, cell refinement, and data reduction. The absorption of raw data sets were corrected for absorption using the multiscan method.<sup>12</sup> The structures were solved using the direct method of structure factor phase retrieval using the software SHELXS-2013<sup>13</sup> and refined by a full-matrix least-squares on  $F^2$  using the software SHELXL-2013.<sup>13</sup> All the asymmetric non-hydrogen atoms were easily found from the electronic density map constructed by Fourier synthesis and refined with anisotropic thermal parameters. The hydrogen atoms bonded to carbons, nitrogens, and hydroxyl oxygens were stereochemically positioned following a riding model with fixed bond lengths of 0.82 Å (O–H), 0.86 Å (N–H in the amide moiety), 0.91 Å (N–H in the N,N-dimethylamine moiety), 0.93 Å (C<sub>sp</sub><sup>2</sup>–H), 0.96 Å (C<sub>sp</sub><sup>3</sup>–H in the methyl groups), and 0.98 Å (C<sub>sp</sub><sup>3</sup>–H in the methine groups). The hydrogen atoms of both the water molecule and the carboxyl group of the acetic acid molecule were assigned based on the residual electron density map. While fractional coordinates of water hydrogens were fixed after assignment using the difference Fourier map, the carboxyl hydrogens of acetic acid were refined freely. Water bond lengths were restrained to 0.85 Å. The

isotropic thermal parameters of all hydrogens depended on the equivalent isotropic thermal displacements of the atoms bonded to them [ $U_{\text{iso}}(\text{H}) = 1.2U_{\text{eq}}(\text{N}, \text{C}_{\text{sp}}^2, \text{C}_{\text{sp}}^3\text{-methine})$  or  $1.5U_{\text{eq}}(\text{O}, \text{C}_{\text{sp}}^3\text{-methyl})$ ]. All three new crystal forms were solved in noncentrosymmetric space groups (Table 1). The absolute configuration was

**Table 1.** Crystallographic Data and Structure Determination Parameters of DOX Crystal Forms Prepared in This Study

	DOX·HCl·2H <sub>2</sub> O	DOX·HAc·2H <sub>2</sub> O	DOX·HNO <sub>3</sub> ·0.5H <sub>2</sub> O
Empirical Formula	C <sub>22</sub> H <sub>29</sub> ClN <sub>2</sub> O <sub>10</sub>	C <sub>24</sub> H <sub>32</sub> N <sub>2</sub> O <sub>12</sub>	C <sub>44</sub> H <sub>52</sub> N <sub>6</sub> O <sub>23</sub>
Formula Weight (g mol <sup>-1</sup> )	516.92	540.52	1032.92
Temperature (K)	293(2)	293(2)	293(2)
Wavelength (Å)	1.54180	0.71073	1.54180
Crystal Size (mm <sup>3</sup> )	0.25 × 0.20 × 0.10	0.25 × 0.15 × 0.12	0.30 × 0.19 × 0.15
Crystal System	Orthorhombic	orthorhombic	triclinic
Space group	P2 <sub>1</sub> 2 <sub>1</sub> 2 <sub>1</sub>	P2 <sub>1</sub> 2 <sub>1</sub> 2 <sub>1</sub>	P1
a (Å)	11.0979(1)	6.4753(2)	8.0679(2)
b (Å)	12.7557(1)	9.0970(4)	8.9156(3)
c (Å)	16.8829(2)	42.8077(16)	16.6791(5)
α (deg)	90	90	77.872(2)
β (deg)	90	90	87.581(2)
γ (deg)	90	90	74.133(3)
Cell Volume (Å <sup>3</sup> )	2389.97(4)	2521.62(17)	1128.11(6)
Z	4	4	1
Calc. density (g cm <sup>-3</sup> )	1.437	1.424	1.520
Absorption coefficient (mm <sup>-1</sup> )	1.945	0.115	1.065
F (000)	1088	1144	542
θ-range (deg)	4.34–62.49	2.86–29.49	2.71–66.37
Index ranges	-12 ≤ h ≤ 12 -14 ≤ k ≤ 14 -19 ≤ l ≤ 19	-7 ≤ h ≤ 8 -12 ≤ k ≤ 10 -57 ≤ l ≤ 55	-8 ≤ h ≤ 9 -10 ≤ k ≤ 10 -19 ≤ l ≤ 19
reflections collected	34212	24360	21480
indep. reflections/R <sub>int</sub>	3799/0.0331	6303/0.0479	7575/0.0283
Completeness to θ <sub>max</sub> (%)	99.4	99.8	98.5
Goodness-of-fit on F <sup>2</sup>	1.050	0.943	1.027
Data/restraints/params.	3786/1/319	6303/0/356	7575/3/662
R1/wR2 for I > 2σ(I)	0.0282/0.0700	0.0432/0.0928	0.0332/0.0840
R1/wR2 for all data	0.0314/0.0721	0.0715/0.0989	0.0369/0.0867
Absolute structure parameter	-0.002(5)	—	0.03(6)
Largest diff. peak/bole (e Å <sup>-3</sup> )	0.138/-0.182	0.194/-0.192	0.441/-0.296

confirmed by XRD methods for DOX·HCl·2H<sub>2</sub>O and DOX·HNO<sub>3</sub>·0.5H<sub>2</sub>O, in which the Cu K $\alpha$  radiation was used to refine the Flack parameter.<sup>14</sup> The absolute configuration of DOX·HCl·2H<sub>2</sub>O was adopted to DOX·HAc·2H<sub>2</sub>O, which is also known for DOX from the synthetic pathway. During the structure determination of DOX·HNO<sub>3</sub>·0.5H<sub>2</sub>O, disordered sites around one of the two nitrate anions present in the asymmetric unit were found. Trial refinements were performed using the split-atom approach for these extra sites. From a statistical and convergence point of view, the classical split-atom model

with two nitrate positions resulted in the best structural refinement. A SHELXL-2013<sup>13</sup> (FVAR instruction) restraint was applied in order to ensure that the site occupation factors of the two disordered nitrates added to unity. The refined free-variable found was 0.598(8), meaning that the relation of the two disordered nitrates was ~60:40 (%).

The software WinGX<sup>15</sup> was used to treat the crystallographic data and generate tables. The MERCURY<sup>16</sup> and ORTEP-3<sup>17</sup> software programs were used for the crystallographic analysis and artwork representations. The crystallographic information was saved as a .cif extension document and the files containing these data (except for structure factors) were deposited in the Cambridge Structural Data Base under deposit codes CCDC 974379, 974380, and 974381 for DOX·HAc·2H<sub>2</sub>O, DOX·HNO<sub>3</sub>·0.5H<sub>2</sub>O, and DOX·HCl·2H<sub>2</sub>O, respectively. Copies of these files may be retrieved free of charge under request (e-mail: deposit@ccdc.cam.ac.uk or http://www.ccdc.ac.uk).

**2.3. Powder X-ray Diffraction Assessments.** The powder X-ray diffraction (PXRD) data were recorded at room temperature (293 K) using a Rigaku Ultima IV diffractometer with  $\theta$ –2 $\theta$  geometry. Cu K $\alpha$  radiation ( $\lambda = 1.5418 \text{ \AA}$ ) was generated using a sealed tube at 40 kV and 30 mA. The data were collected with a step size of 0.02°. The count time was 0.5 s/step from 3° to 35° in 2 $\theta$ . The samples were finely ground and mounted on a grooved glass slide employed as a sample holder. These experimental X-ray powder diffractograms were compared to the corresponding theoretical diffractograms simulated using MERCURY<sup>16</sup> by inputting the final CIF files obtained from refinement of the single-crystal X-ray diffraction data for each solid. The crystal structures of DOX·HCl·2H<sub>2</sub>O, DOX·HNO<sub>3</sub>·0.5H<sub>2</sub>O, and DOX·HAc·2H<sub>2</sub>O that are reported here and the structures of DOX·H<sub>2</sub>O and DOX·HYC that we previously reported<sup>8</sup> were used. The PXRD simulation conditions were set to be identical to the experimental conditions.

**2.4. Thermal Analysis.** Differential scanning calorimetry (DSC) measurements were performed on a DSC Calorimeter (model DSC7020, SII Nano Technology, Japan) using hermetic aluminum crucibles for the samples and references. Samples masses of approximately 3 mg were heated at a rate of 10 °C min<sup>-1</sup> under a nitrogen air atmosphere of 50 mL min<sup>-1</sup>. Thermogravimetric (TG) curves were obtained on a thermobalance (model TG/DTA7300, SII Nano Technology, Japan) using open aluminum crucibles, a heating rate of 10 °C min<sup>-1</sup>, nitrogen at a 50 mL min<sup>-1</sup> flow, and samples of approximately 4 mg.

**2.5. Infrared Analysis.** ATR/FTIR spectra were obtained using an Affinity-1 Fourier Transform infrared spectrophotometer (ShimadzuTM, Tokyo, Japan) coupled to a Pike Miracle attenuated total reflectance sampling accessory with ZnSe waveguides (Pike Technologies, Madison, Wisconsin, USA). Spectra were recorded at room temperature in the 4000–600 cm<sup>-1</sup> range. After recording a background spectrum, the samples were placed on the crystal. 32 scans were recorded from each sample with a resolution of 4 cm<sup>-1</sup>.

**2.6. Spectrophotometric Measurements and Calibration Curves.** A Shimadzu model 1800 (Kyoto, Japan) UV visible spectrophotometer connected to a computer loaded with Shimadzu UVPORBE v 3.9 software was used.

The spectra for each DOX form were built in the range from 400 to 200 nm using 1 cm quartz cuvettes in the fast scan speed at a 2.0 nm data interval and 2 nm bandwidth (Figure S1, Supporting Information). After this, the wavelengths chosen for analysis were 268 nm for DOX·H<sub>2</sub>O and 274 nm for DOX·HYC, DOX·HCl·2H<sub>2</sub>O, DOX·HNO<sub>3</sub>·0.5H<sub>2</sub>O, and DOX·HAc·2H<sub>2</sub>O.

The calibration curves were prepared from a stock solution of each DOX form in distilled water at six concentration levels in five replications (7, 10, 15, 20, 25, and 30 μg mL<sup>-1</sup>). DOX·H<sub>2</sub>O was solubilized in 0.1 mol L<sup>-1</sup> hydrochloric acid, followed by dilution in distilled water. The regression equations for the calibration curves were found to be  $y = 0.0398x - 0.0108$ , with a correlation coefficient ( $r$ ) of 0.9998 for DOX·H<sub>2</sub>O;  $y = 0.0308x - 0.0065$  with  $r$  of 0.9998 for DOX·HYC;  $y = 0.030x + 0.003$  with  $r$  of 0.9999 for DOX·HCl·2H<sub>2</sub>O;  $y = 0.0314x - 0.0089$  with  $r$  of 0.9998 for DOX·HNO<sub>3</sub>·0.5H<sub>2</sub>O; and  $y = 0.028x + 0.001$  with  $r$  of 0.9999 for DOX·HAc·2H<sub>2</sub>O.

**2.7. Equilibrium Solubility.** The solubility test was determined using the equilibrium method. DOX·H<sub>2</sub>O, DOX·HYC, DOX·HCl·2H<sub>2</sub>O, DOX·HNO<sub>3</sub>·0.5H<sub>2</sub>O, and DOX·HAc·2H<sub>2</sub>O were added in excess to 1.5 mL Eppendorf tubes containing 1 mL total volume of the following solution: ultrapure water, 0.1 mol L<sup>-1</sup> HCl, 0.01 mol L<sup>-1</sup> HCl, pH 4.5 acetate buffer, pH 5.8 potassium phosphate buffer, pH 6.8 potassium phosphate buffer, and pH 7.5 potassium phosphate buffer. The solutions were prepared in triplicate. Subsequently, the flasks were protected from light and agitated at 150 rpm at room temperature (25 ± 2 °C) on a SolabTM model SL 180 DT shaker table (Piracicaba, São Paulo, Brasil). After 48 h stirring, the samples were filtered on PTFE hydrophilic filters (13 mm diameter, 0.50 μm porosity, Advantec MSF, Dublin, CA, USA). The final pH of each solution was measured before solutions were diluted with water. The concentration of DOX forms in each solvent was determined by the UV method using the calibration curve for each form (section 2.6). The undissolved solid materials were dried in a desiccator containing silica for 5 days, after which time they were analyzed by PXRD to verify if the resulting material was the same as the starting material.

**2.8. Chromatographic Conditions and Calibration Curves.** The samples were quantified for forced degradation studies with a stability-indicating UV-HPLC method.<sup>18</sup> Chromatographic separations were carried out using a ShimadzuTM HPLC system series LC-10A (Kyoto, Japan). The following chromatographic parameters were used: Shim-pack CLC-ODS column (250 mm × 4.6 mm i.d., 5.0 μm particle size), ShimadzuTM (Kyoto, Japan) at 25 °C as stationary phase, water/acetonitrile/perchloric acid (74:26:0.25 v/v/v) adjusted to pH 2.5 with 5 mol L<sup>-1</sup> sodium hydroxide at a flow rate of 1 mL min<sup>-1</sup> as the mobile phase, and UV detection at 350 nm. Twenty microliters of sample was injected into the HPLC system.

The calibration curves were prepared from a stock solution of each DOX form in mobile phase at five concentration levels in triplicate (10, 20, 30, 40, and 50 μg mL<sup>-1</sup>). The peak area vs concentration data were analyzed using least-squares linear regression. The obtained regression equation was used to quantify the DOX forms before performing the forced degradation studies.

The regression equations for the calibration curves were found to be as follows:  $y = 21461x - 20806$  with a correlation coefficient ( $r$ ) of 0.9977 for DOX·H<sub>2</sub>O;  $y = 19465x - 56176$  with  $r$  of 0.9989 for DOX·HYC;  $y = 19193x - 51172$  with  $r$  of 0.9993 for DOX·HCl·2H<sub>2</sub>O;  $y = 19263x - 63336$  with a  $r$  of 0.9977 for DOX·HNO<sub>3</sub>·0.5H<sub>2</sub>O; and  $y = 20705x - 99613$  with a  $r$  of 0.9990 for DOX·HAc·2H<sub>2</sub>O.

**2.9. Forced Degradation Studies.** Forced degradation studies were performed to compare the stability of DOX forms according to the International Conference on Harmonization (ICH) guidance.

**2.9.1. Oxidation, Acid, Alkali, and Neutral Degradation Studies.** The DOX forms at a concentration of 400.0 μg mL<sup>-1</sup> were used in all degradation studies. The samples were subjected to stress conditions in 1% hydrogen peroxide, 0.01 mol L<sup>-1</sup> HCl, 0.01 mol L<sup>-1</sup> NaOH, and water at 60 °C in oven for 12 h. The blank solutions were treated similarly. These solutions were neutralized, diluted with mobile phase to obtain a solution with a concentration of 40 μg mL<sup>-1</sup> of DOX forms, and filtered through a 0.45 μm PTFE-membrane filter (Millipore, Bedford, USA) prior to injection into the HPLC system (Section 2.8). Corresponding blanks were simultaneously injected.

**2.9.2. Photostability.** For the photostability studies, 100 mg of each DOX form were exposed to UV light for 7 days to evaluate the effects of light irradiation on the stability of previously sieved DOX forms. After the test, 10 mg was weighed and transferred into a 25 mL volumetric flask. Approximately 20 mL of mobile phase was added and sonicated for 5 min. The volume was completed with mobile phase and a further dilution of 1 mL was added to a 10 mL volumetric flask, yielding a final concentration of 40 μg mL<sup>-1</sup>. The obtained solutions were filtered through a 0.45 μm PTFE-membrane filter (Millipore, Bedford, USA) and injected into the HPLC system (section 2.8). The PXRD analyses of samples were performed before and after exposure to UV light.

**2.10. Preparation of DOX Forms in Capsules.** In order to evaluate the influence of DOX forms on capsules, batches with 30 capsules containing DOX forms as APIs were prepared as follows: 100

mg of each sieved DOX form was added to a 50 mg portion of the placebo test mixture. These substances were mixed in an aluminum container by vigorous shaking and the batches were obtained by manually filling size 4 hard gelatin capsules with the mixture (API + excipients). The placebo mixture contained the following inactive excipients: magnesium stearate (0.8%), colloidal silicon dioxide (0.2%), sodium starch glycolate (4.0%), and microcrystalline cellulose (95.0%). This formulation contains the same excipients contained in the commercial DOX·H<sub>2</sub>O capsules produced by RANBAXY Pharmaceutical Industry.

**2.11. Dissolution Profiles.** Solid pharmaceutical products such as capsules must release the drug in appropriate amounts and rates in order to achieve therapeutic effects. In vitro dissolution testing is widely used to evaluate the drug release from the drug product and to predict the in vivo absorption and bioavailability of the drug.

In this test, six capsules of each DOX form and one containing only the inactive excipients (as the blank) were evaluated an ElectrolabTM TDT-08 L multi bath ( $n = 8$ ) dissolution test system (Mumbai, Maharashtra, India). The capsules were placed in sinkers (stainless steel wire) to avoid capsule fluctuation. The dissolution experimental conditions were 1000 mL of 6.8 phosphate buffer as the dissolution medium and a paddle stirrer as the apparatus, stirring at a rate of 100 rpm. The assays were performed according to U.S. Pharmacopoeia but we altered the dissolution medium (water) to pH 6.8 phosphate buffer in order to simulate the pH of the water and to prevent pH changes during testing. Five milliliters of dissolution medium (controlled at 37.0 ± 0.5 °C) were sampled after 3, 6, 9, 15, 20, and 30 min and were immediately replaced. The sample aliquots were diluted with water when necessary and using the UV method (section 2.6). The last sampling point was taken at 30 min because the USP<sup>20</sup> recommends procedure duration of 30 to 60 min for immediate release dosage forms. After this, comparisons of the dissolution profiles were performed. The similarity of the dissolution profiles was determined by a similarity factor (F2), calculated from eq 1 as follows:

$$F2 = 50 \times \log \left\{ \left[ (1 + 1/n) \sum_{t=1}^n (R_t - T_t)^2 \right]^{-0.5} \times 100 \right\} \quad (1)$$

where  $R_t$  is the percentage of reference drug dissolved at each time point,  $T_t$  is the percentage of test product dissolved at each time point, and  $n$  is the number of sampling time points. For curves to be considered similar, F2 values had to be close to 100. Generally, F2 values greater than 50 (i.e., 50–100) ensured the equivalence of the two curves.<sup>21,22</sup>

### 3. RESULTS AND DISCUSSION

**3.1. Intramolecular Structures: Fused Keto–Enol Rings.** Both DOX·HCl·2H<sub>2</sub>O and DOX·HAc·2H<sub>2</sub>O crystallize in the higher-symmetry orthorhombic  $P2_12_12_1$  space group with two water molecules and only one drug molecule in the asymmetric unit (Figure S2, Supporting Information). Another similarity between them resides in the formation of two fused  $S_1^1(6)$  intramolecular rings,<sup>23</sup> as observed in the literature regarding DOX·H<sub>2</sub>O and DOX·HYC crystals (Figure S2, Supporting Information). An enlarged C10=O2 bond (larger than 1.22 Å, an expected carbonyl bond length; see Table S1, Supporting Information) is also reported for all structures described here (including both the crystallographically independent molecules of DOX·HNO<sub>3</sub>·0.5H<sub>2</sub>O) and in previously described structures. This is a consequence of RAHB in both  $S_1^1(6)$  rings that increases the single bond character of C10=O2 carbonyl due to the electronic delocalization of π-bonds along O2–C10–C6–C1–O1 and along O2–C10–C9–C14–O3. The conjugation in both keto–enol moieties is stated based on the increased planarity of the atoms onto the least-squares planes calculated through each  $S_1^1(6)$  ring. This is shown by the following: (1) the low values of

torsions around C6–C10 and C9–C10 bonds; (2) the largest deviation from the least-squares plane; (3) the r.m.s. deviation of fitted atoms; and (4) the low angle between the O2–C10–C6–C1–O1 and O2–C10–C9–C14–O3 planes (Table S2, Supporting Information). One can observe, however, that the enlargement of the C10=O2 bond length is not as pronounced in DOX·HAc·2H<sub>2</sub>O as in the other crystal forms (Table S1, Supporting Information). This arises from decreased conjugation encompassing O2–C10–C6–C1–O1 in this structure, as noted by the largest values of the aforementioned planarity indicators. Therefore, resonance-assistance to the intramolecular O1–H1…O2 HB is prevented. This phenomenon is rationalized by the intermolecular O12–H12b…O1 (Figure 2), in which the hydroxyl O1 oxygen is pulled toward

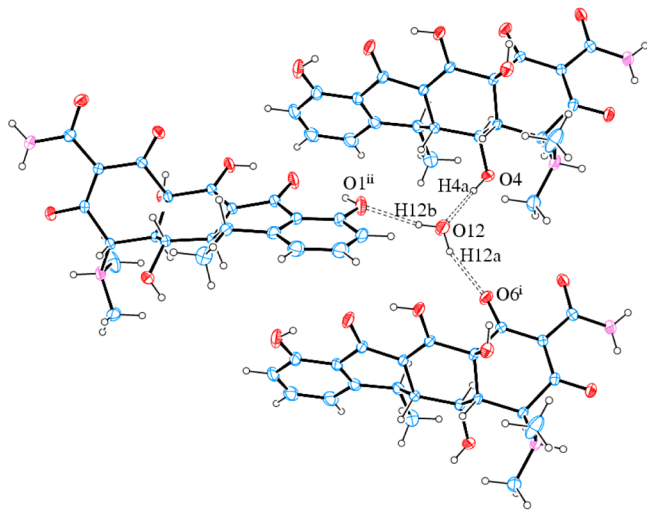


**Figure 2.** Water-DOX HB pattern in DOX·HAc·2H<sub>2</sub>O is as occurs in DOX·2H<sub>2</sub>O. Symmetry transformations: (i) ( $x, y + 1, z$ ) and (ii) ( $-x + 1, y + 0.5, -z + 0.5$ ).

the O12–H12b HB donor group of one water molecule. Indeed, the O2–C10–C6–C1–O1 moiety is less resonant than O2–C10–C9–C14–O3 in all known DOX crystal forms and in those reported here except DOX·HNO<sub>3</sub>·0.5H<sub>2</sub>O T1 (this is noted by the planarity descriptors given in Table S2, Supporting Information). Table S2 shows that DOX·HCl·2H<sub>2</sub>O is present with the highest angle between the O2–C10–

C6–C1–O1 and O2–C10–C9–C14–O3 planes, which is a consequence of the intermolecular O4–H4a…O3 HB (Figure 3).

DOX·HCl·2H<sub>2</sub>O and DOX·HAc·2H<sub>2</sub>O do not have an adjacent S<sub>i</sub><sup>1</sup>(5) ring to the fused S<sub>i</sub><sup>1</sup>(6) rings. This is in contrast to both the previously crystal forms and the two tautomers of DOX·HNO<sub>3</sub>·0.5H<sub>2</sub>O (see Figure S3 in Supporting Information and geometrical parameters for O5–H5…O3 HB in Table 2). In this way, the previously reported S<sub>3</sub><sup>2</sup>(13) intramolecular pattern for the DOX molecule is only observed in one of the three crystal phases described here. In the two others, O5–H5 hydroxyl is a HB donor to either chloride (O5–H5…Cl1 in DOX·HCl·2H<sub>2</sub>O, Figure 4) or one water oxygen (O5–H5…O11 in DOX·HAc·2H<sub>2</sub>O, Figure 5). The geometric parameters of the classical intra- and intermolecular HB in the DOX·HCl·2H<sub>2</sub>O and DOX·HAc·2H<sub>2</sub>O structures are given in Table 2.

**3.2. Intramolecular Structures: Keto–Enolate Tautomerism and Amide Moiety Conformation.** The similarities between DOX·HCl·2H<sub>2</sub>O and DOX·HAc·2H<sub>2</sub>O noted in the previous section end there. In addition to one chloride anion and one acetic acid molecule (HAc) in their asymmetric unit (Figure S2, Supporting Information), respectively, these two compounds differ in their protonation patterns, major tautomers, and conformation of their amide moieties. DOX has a net positive charge in DOX·HCl·2H<sub>2</sub>O, in which there are two positive charges on N1 and O8 and one negative charge on O7. Therefore, the *N,N*-dimethylamine and amide carbonyl groups are protonated while the nearby hydroxyl moiety undergoes deprotonation. Protonation of the amide carbonyl oxygen is rarely found in the crystals of small molecules. There are only 33 entries for a protonated oxygen of an amide moiety in the CSD (version 5.35 updated in November 2013, 658,007 entries).<sup>24</sup> In most entries (22), strong acids such as perchloric, hydrochloric, hydrobromic, nitric, or sulfuric acids are crystallized together. This reflects that a proton is mainly transferred to the amide carbonyl oxygen in the presence of strong acids, as occurs in the salts with the same protonation pattern described in this study. The net positive charge on DOX that results in chloride and nitrate salts according to the pK<sub>a</sub> rule will also be discussed later in this section.<sup>25,26</sup> The formation of an intramolecular hydrogen-bonded keto–enol ring occurs in six entries in which strong acids are absent. This also occurs in our salts and helps explain the proton transfer in those known structures. Therefore, both issues support the protonation of

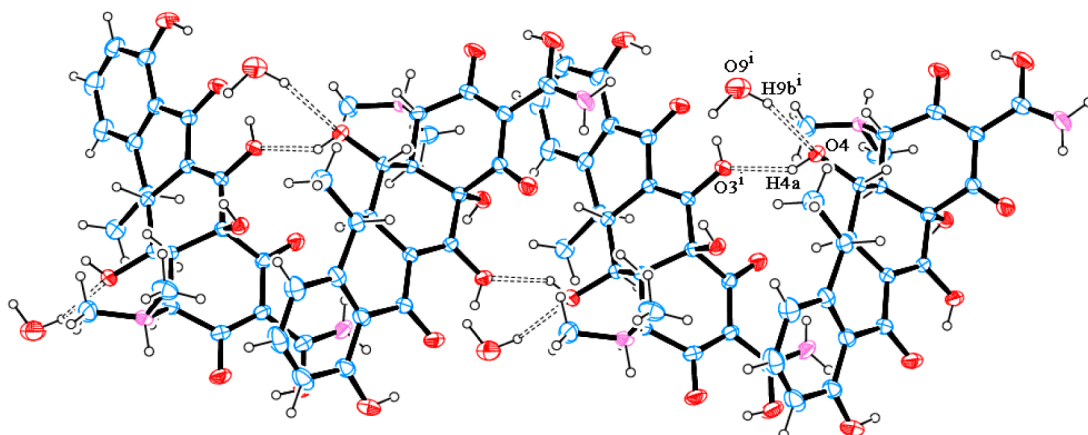


**Figure 3.** HB that connects DOX molecules along the [010] direction in DOX·HCl·2H<sub>2</sub>O. Interaction between water and DOX molecules is also shown. Symmetry transformation: (i) ( $-x + 1, y - 0.5, -z + 1.5$ ).

**Table 2. Distances and Angles of Inter- and Intramolecular HB Present in the Crystal Structure of DOX·HNO<sub>3</sub>·0.5H<sub>2</sub>O, DOX·HCl·2H<sub>2</sub>O, and DOX·HAc·2H<sub>2</sub>O<sup>a</sup>**

		D	H	A	D–H (Å)	H···A (Å)	D···A (Å)	D–H···A (deg)
DOX·HNO <sub>3</sub> ·0.5H <sub>2</sub> O	INTRA	O1	H1	O2	0.82	1.84	2.563(3)	146
		O1'	H1'	O2'	0.82	1.81	2.536(3)	147
		O3	H3a	O2	0.82	1.72	2.453(2)	147
		O3'	H3a'	O2'	0.82	1.82	2.533(2)	145
		O5	H5	O3	0.82	2.26	2.688(3)	113
		OS'	HS'	O3'	0.82	2.63	2.688(3)	109
		O8	H8a	O6	0.82	1.69	2.688(3)	152
		O8'	H8a'	O7'	0.82	1.70	2.452(3)	152
		N2	H2b	O7	0.86	2.18	2.806(3)	129
		N2'	H2b'	O6'	0.86	2.09	2.724(3)	130
	INTER	O4'	H4a'	O13	0.82	2.00	2.795(4)	164
		O4'	H4a'	O15'	0.82	2.28	2.953(4)	140
		O4	H4a	O10 <sup>b</sup>	0.82	2.35	3.128(4)	159
		O5	H5	O10	0.82	2.04	2.818(3)	160
		O12	H12b	O11 <sup>c</sup>	0.99	1.88	2.861(3)	171
		O12	H12a	O15 <sup>d</sup>	0.99	1.98	2.892(4)	171
		O12	H12a	O15 <sup>e</sup>	0.99	2.10	2.950(4)	153
		N1	H1a	O12	0.91	1.89	2.735(3)	154
		N1'	H1a'	O11 <sup>f</sup>	0.86	1.97	2.816(3)	154
		N2	H2a	O14 <sup>d</sup>	0.86	2.08	2.932(3)	174
		N2	H2a	O14 <sup>e</sup>	0.86	2.22	2.896(3)	135
		D	H	A	D–H (Å)	H···A (Å)	D···A (Å)	D–H···A (deg)
DOX·HCl·2H <sub>2</sub> O	INTRA	O1	H1	O2	0.82	1.89	2.609(2)	146
		O3	H3a	O2	0.82	1.74	2.468(2)	148
		O8	H8a	O7	0.82	1.69	2.445(2)	152
		N2	H2b	O6	0.86	2.12	2.751(2)	130
		O4	H4a	O3 <sup>f</sup>	0.82	2.07	2.797(2)	148
		O5	H5	Cl1	0.82	2.20	3.012(2)	171
		O9	H9a	Cl1	1.00	2.21	3.194(2)	168
		O9	H9b	O4 <sup>g</sup>	0.87	2.30	3.054(2)	144
		O10	H10a	Cl1 <sup>h</sup>	0.87	2.30	3.157(2)	165
		O10	H10b	O9 <sup>f</sup>	0.85	2.05	2.884(2)	168
	INTER	N1	H1a	O10 <sup>i</sup>	0.91	2.21	3.019(2)	147
		N2	H2a	O10	0.86	2.06	2.901(2)	165
		N2	H2b	Cl1 <sup>f</sup>	0.86	2.65	3.240(2)	127
		D	H	A	D–H (Å)	H···A (Å)	D···A (Å)	D–H···A (deg)
		O1	H1	O2	0.82	1.87	2.577(3)	144
DOX·HAc·2H <sub>2</sub> O	INTRA	O3	H3a	O2	0.82	1.79	2.504(2)	145
		N2	H2b	O7	0.86	1.98	2.647(3)	134
		O4	H4a	O12	0.82	1.92	2.740(4)	176
		O5	H5	O11	0.82	1.92	2.738(3)	171
		O9	H9	O8	0.97(4)	1.63(4)	2.553(3)	159(3)
		O11	H11b	O6 <sup>j</sup>	0.85	2.50	2.900(3)	110
		O11	H11b	O8 <sup>j</sup>	0.85	1.99	2.832(3)	169
		O12	H12a	O6 <sup>k</sup>	0.85	1.98	2.763(3)	154
		O12	H12b	O1 <sup>l</sup>	0.85	2.07	2.906(4)	168
		N1	H1a	O10 <sup>m</sup>	0.91	2.08	2.873(3)	145
	INTER	N2	H2a	O10	0.86	2.28	3.050(3)	149

<sup>a</sup>The donor and acceptor atoms are referred to by “D” and “A”, respectively. Symmetry transformations used to generate equivalent atoms are as in the following footnotes. <sup>b</sup>(*x*, *y* – 1, *z*). <sup>c</sup>(*x* + 1, *y* – 1, *z*). <sup>d</sup>(*x*, *y*, *z* – 1). <sup>e</sup>(*x*, *y* – 1, *z* + 1). <sup>f</sup>(–*x* + 1, *y* – 0.5, –*z* + 1.5). <sup>g</sup>(–*x* + 1, *y* + 0.5, –*z* + 1.5). <sup>h</sup>(–*x* + 1.5, –*y* + 2, *z* – 0.5). <sup>i</sup>(–*x* + 2, *y* – 0.5, –*z* + 1.5). <sup>j</sup>(*x* + 1, *y*, *z*). <sup>k</sup>(*x*, *y* + 1, *z*). <sup>l</sup>(–*x* + 1, *y* + 0.5, –*z* + 0.5). <sup>m</sup>(*x* + 0.5, –*y* + 0.5, –*z* + 1).

amide oxygen in the salts reported here. Intermolecular motifs assembled with a protonated amide oxygen as the HB donor occur in the other four structures when strong acids are not present.

The enolate tautomer between C16=C17 and O7<sup>-</sup> occurs in the T1 tautomers of both DOX·HNO<sub>3</sub>·0.5H<sub>2</sub>O and DOX·HYC. In addition, the T1 tautomers of DOX·HNO<sub>3</sub>·0.5H<sub>2</sub>O

and DOX·HYC are similar to those of DOX·HCl·2H<sub>2</sub>O in terms of protonation pattern and amide group conformation. In the T1 tautomers of DOX·HNO<sub>3</sub>·0.5H<sub>2</sub>O, DOX·HCl·2H<sub>2</sub>O, and DOX·HYC, two fused S<sub>1</sub><sup>1</sup>(6) intramolecular rings give rise to an S<sub>2</sub><sup>2</sup>(10) array (Figures S2 and S3, Supporting Information). One of these S<sub>1</sub><sup>1</sup>(6) rings is assembled through the O8–H8A···O7 RAHB, as shown by the strong double-bond

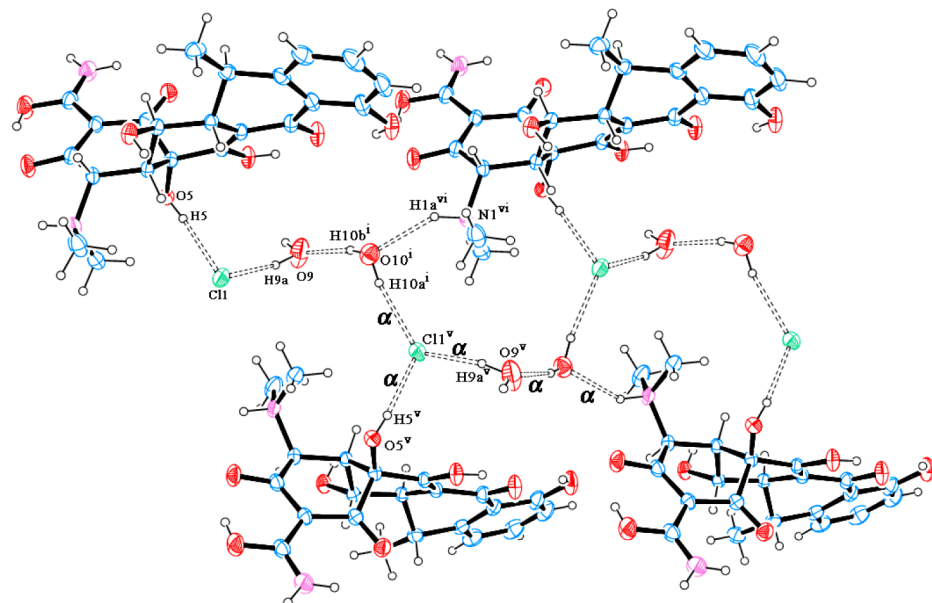


**Figure 4.** Organization of DOX-chloride ionic pairs into a  $C_5^3(11)$  chain assembled with the set of  $\alpha$ -labeled HB in DOX·HCl·2H<sub>2</sub>O. Each chain grows parallel to the [100] direction. Symmetry transformations: (i)  $(-x + 1, y - 0.5, -z + 1.5)$ , (v)  $(x - 0.5, -y + 1.5, -z + 2)$ , and (vi)  $(x - 1, y, z)$ .

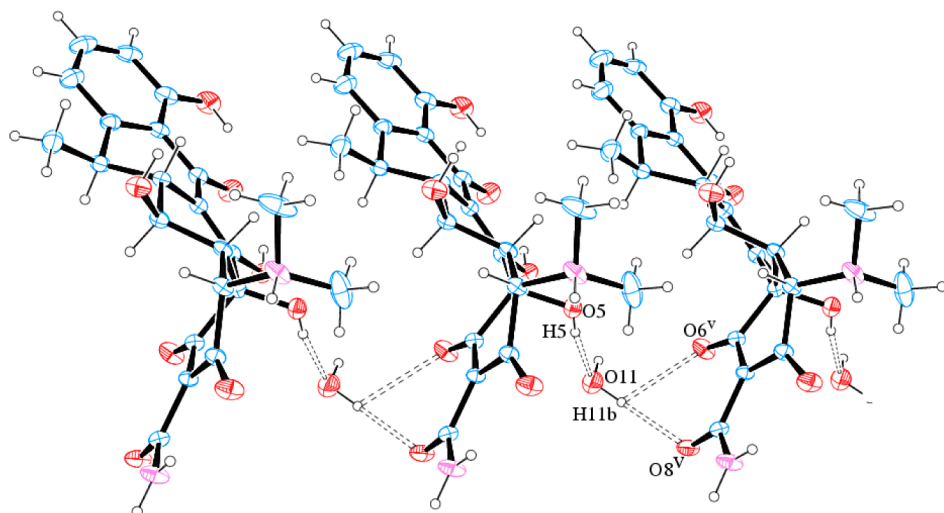


**Figure 5.** HB between one of two crystallographically independent water molecules and translation-symmetry related DOX units along the [100] direction in DOX·HAc·2H<sub>2</sub>O. Symmetry transformation: (v)  $(x + 1, y, z)$ .

character of the C16—O7 and C17—C20 single bonds and by the remarkable single-bond character of the C16=C17 and C20=O8 double bonds. For DOX·HCl·2H<sub>2</sub>O and the T1 tautomers of DOX·HNO<sub>3</sub>·0.5H<sub>2</sub>O and DOX·HYC, the C16—O7 and C17—C20 bond lengths were shorter than those expected for single  $C_{sp}^2$ —O and  $C_{sp}^2$ —C<sub>sp</sub><sup>2</sup> bonds (ca. 1.36 and 1.48 Å, respectively). On the contrary, an opposite trend of enlargement was observed for C16=C17 and C20=O8 bond lengths. This reflects the strong  $\pi$ -electron delocalization across O7—C16—C17—C20—O8. The other  $S_1^1(6)$  intramolecular motif along O6—C18—C17—C20—N2—H2B is not resonance-assisted because the C18=O6 and C17—C18 bond lengths agree well with the expected values for a carbonyl double bond and a  $C_{sp}^2$ —C<sub>sp</sub><sup>2</sup> single bond.

The T2 tautomers of DOX·HNO<sub>3</sub>·0.5H<sub>2</sub>O and DOX·HYC resemble each other, as C17=C18 and O6<sup>-</sup> are present with two fused  $S_1^1(6)$  intramolecular rings in a  $S_2^2(10)$  pattern in both

structures (Figure S3, Supporting Information). However, there is a rotation of ca. 180° on the C17—C20 bond axis if the amide bridge of T1 is taken as a reference. The amide moiety conformation differs for both the tautomers of DOX·HNO<sub>3</sub>·0.5H<sub>2</sub>O. This is likewise observed for the two tautomers of DOX·HYC. The T1 tautomers are present with the same amide group conformation in DOX·HNO<sub>3</sub>·0.5H<sub>2</sub>O and DOX·HYC. An overlay of the  $S_2^2(10)$  motif and its neighbors is shown in Figure S4 (a) (Supporting Information) for these tautomers. The conformational similarity between DOX·HNO<sub>3</sub>·0.5H<sub>2</sub>O and DOX·HYC for the amide moiety of their T2 tautomers is also depicted in Figure S4 (b) (Supporting Information).

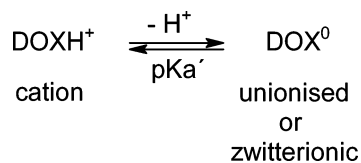
This amide group conformation is responsible for the formation of a RAHB with an  $S_1^1(6)$  motif. However, unlike T1, the  $\pi$ -electron delocalization encompasses the O6—C18—C17—C20—O8 moiety in T2 as shown by the noticeable double-bond character of C18=O6 and C17—C20 single bonds

and the single-bond feature of the C17=C18 and C20=O8 double bonds (Table S1, Supporting Information). The C16=O7 and C16-C17 bond lengths do not deviate considerably from expected values. Therefore, the other S<sub>i</sub><sup>1</sup>(6) motif assembled over O7-C16-C17-C20-N2-H2B is not resonance-assisted in T2.

The C20–N2 bond length of the three salt forms (DOX·HNO<sub>3</sub>·0.5H<sub>2</sub>O, DOX·HCl·2H<sub>2</sub>O, and DOX·HYC) is notably shorter than the same bond in neutral DOX·HAc·2H<sub>2</sub>O and DOX·H<sub>2</sub>O molecules. This reflects a resonance phenomenon in the protonated amide moiety along the N2–C20–O8 atoms that attempts to stabilize the positive charge in both  $\pi$ -electron rich atoms. However, it is important to note that this electronic conjugation is clearly not extended toward the carbonyl group neighboring the amide group, as discussed above.

In contrast to DOX-HCl·2H<sub>2</sub>O, DOX-HNO<sub>3</sub>·0.5H<sub>2</sub>O, and DOX-HYC, in which DOX is cationic, the drug molecule is neutral in DOX-HAc·2H<sub>2</sub>O and in the previously identified DOX·H<sub>2</sub>O. Thus, the proton remains linked to the acetate acid in the crystal and consequently the amide carbonyl group does not present the additional proton, which would lead to cationic DOX. The protonation–deprotonation equilibria of DOX enables two DOX species to exist in solutions with an acidic or neutral pH (Scheme 1). The pK<sub>a</sub> for protonation of DOX (DOX<sup>0</sup> + H<sup>+</sup> → DOXH<sup>+</sup>) was determined to be 3.09 ( $\mu = 1$  and 25 °C).<sup>27</sup>

### Scheme 1



Either protonated or deprotonated DOX can also occur in multicomponent crystalline forms containing DOX. According to the  $pK_a$  rule,<sup>25,26</sup> the salt formation is expected for DOX·HCl·2H<sub>2</sub>O, DOX·HNO<sub>3</sub>·0.5H<sub>2</sub>O, and DOX·HYC because their respective  $\Delta pK_a$  ( $\Delta pK_a = pK_a[\text{protonated base}] - pK_a[\text{acid}]$ ) are greater than 4 ( $\Delta pK_a_{\text{DOX}\cdot\text{HCl}\cdot 2\text{H}_2\text{O}} =$

$\Delta pK_{\text{aDOX-HYC}} = pK_{\text{aDOX}} - pK_{\text{aHCl}} = 3.09 - (-7) = 10.09$ ;  $\Delta pK_{\text{aDOX-HNO}_3 \cdot 0.5\text{H}_2\text{O}} = pK_{\text{aDOX}} - pK_{\text{aHNO}_3} = 3.09 - (-1.34) = 4.43$ ). This is a so-called  $\Delta pK_a$  zone 3<sup>26</sup> in which crystal structures containing ionized A B<sup>+</sup> pairs are almost exclusively observed.<sup>26</sup> On the other hand, for DOX-HAc-2H<sub>2</sub>O, the  $\Delta pK_a$  ( $pK_{\text{aDOX}} - pK_{\text{aHAC}} = 3.09 - 4.76 = -1.67$ ) is in zone 1 ( $\Delta pK_a < -1$ ), where crystal structures containing nonionized AB pairs are almost exclusively observed.<sup>26</sup>

Independent of being un-ionized or ionized, all DOX forms are zwitterionic in the solid state because their N1 atoms are protonated and one hydroxyl moiety undergoes deprotonation. This forms the cationic/zwitterionic specie  $\text{DOXH}^{2+}$  (net charge 1+) for  $\text{DOX}\cdot\text{HCl}\cdot 2\text{H}_2\text{O}$ ,  $\text{DOX}\cdot\text{HNO}_3\cdot 0.5\text{H}_2\text{O}$ , and  $\text{DOX}\cdot\text{HYC}$  and the neutral/zwitterionic specie  $\text{DOX}^{\pm}$  (net charge 0) for  $\text{DOX}\cdot\text{HAc}\cdot 2\text{H}_2\text{O}$  and  $\text{DOX}\cdot 2\text{H}_2\text{O}$ . The chemical diagrams shown in Figure S5 (Supporting Information) summarize the protonation patterns, keto–enolate tautomers, and amide conformers found in each DOX crystal form.

Though DOX-HAc·2H<sub>2</sub>O and DOX·2H<sub>2</sub>O are both neutral/zwitterionic in the crystal, their DOX forms differ for their major tautomer (Figure S5, Supporting Information). While a T2-like enolate tautomer with C17=C18 and O6<sup>-</sup> appears in the corresponding monohydrate form, DOX-HAc·2H<sub>2</sub>O forms a C17=C16—O7<sup>-</sup> enolate tautomer similar to T1 of both DOX·HNO<sub>3</sub>·0.5H<sub>2</sub>O and DOX-HYC.

Another similarity between DOX·HAc·2H<sub>2</sub>O and DOX·H<sub>2</sub>O exists in the formation of the S<sub>1</sub><sup>1</sup>(6) cycle between the enolate oxygen and amide NH<sub>2</sub> (Figure S2, Supporting Information). Based on the bond length analysis of the amide moiety and its neighbors, it is possible to conclude that this S<sub>1</sub><sup>1</sup>(6) motif is not resonance-assisted in either structure because the strong single-bond character of C17–C20 instead of a higher bond order is expected as a consequence of  $\pi$ -electron delocalization. Importantly, this intramolecular hydrogen-bonded cycle is made up of O7–C16–C17–C20–N2–H2B atoms in DOX·HAc·2H<sub>2</sub>O and O6–C18–C17–C20–N2–H2B in DOX·H<sub>2</sub>O due to the conformation of the amide moiety. Intramolecular inspection indicates a rotation of approximately 180° around the C17–C20 bond axis, which places the NH<sub>2</sub> HB donor in the direction of the enolate oxygen (O7 in DOX·HAc·2H<sub>2</sub>O and O6 in DOX·H<sub>2</sub>O). The amide carbonyl bond length is

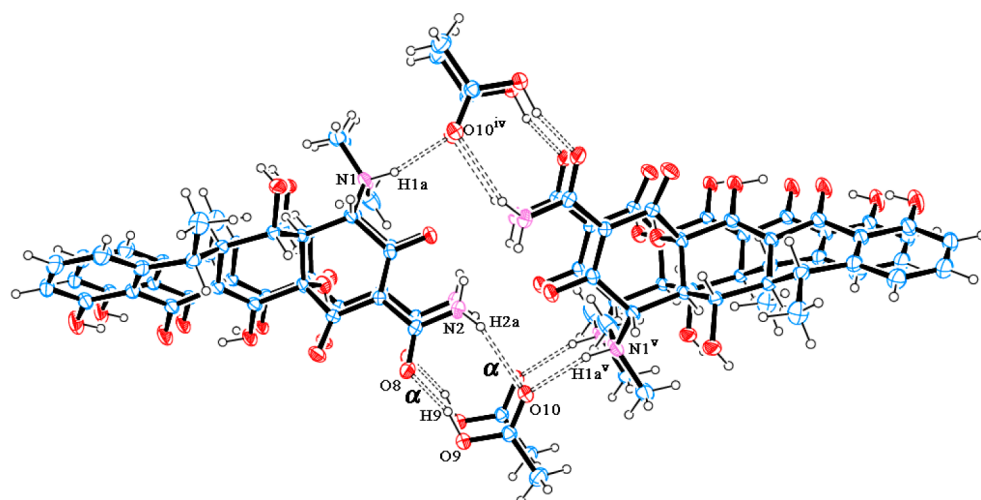


**Figure 6.**  $R_2^2(8)$ -assembled DOX-HAc pairs and their packing along the [100] direction in DOX-HAc- $2\text{H}_2\text{O}$ .  $\alpha$ -Labeled HBs refer to the intermolecular  $R_2^2(8)$  ring. Symmetry transformations: (iv)  $(x + 0.5, -y + 0.5, -z + 1)$  and (v)  $(x - 0.5, -y + 0.5, -z + 1)$ .

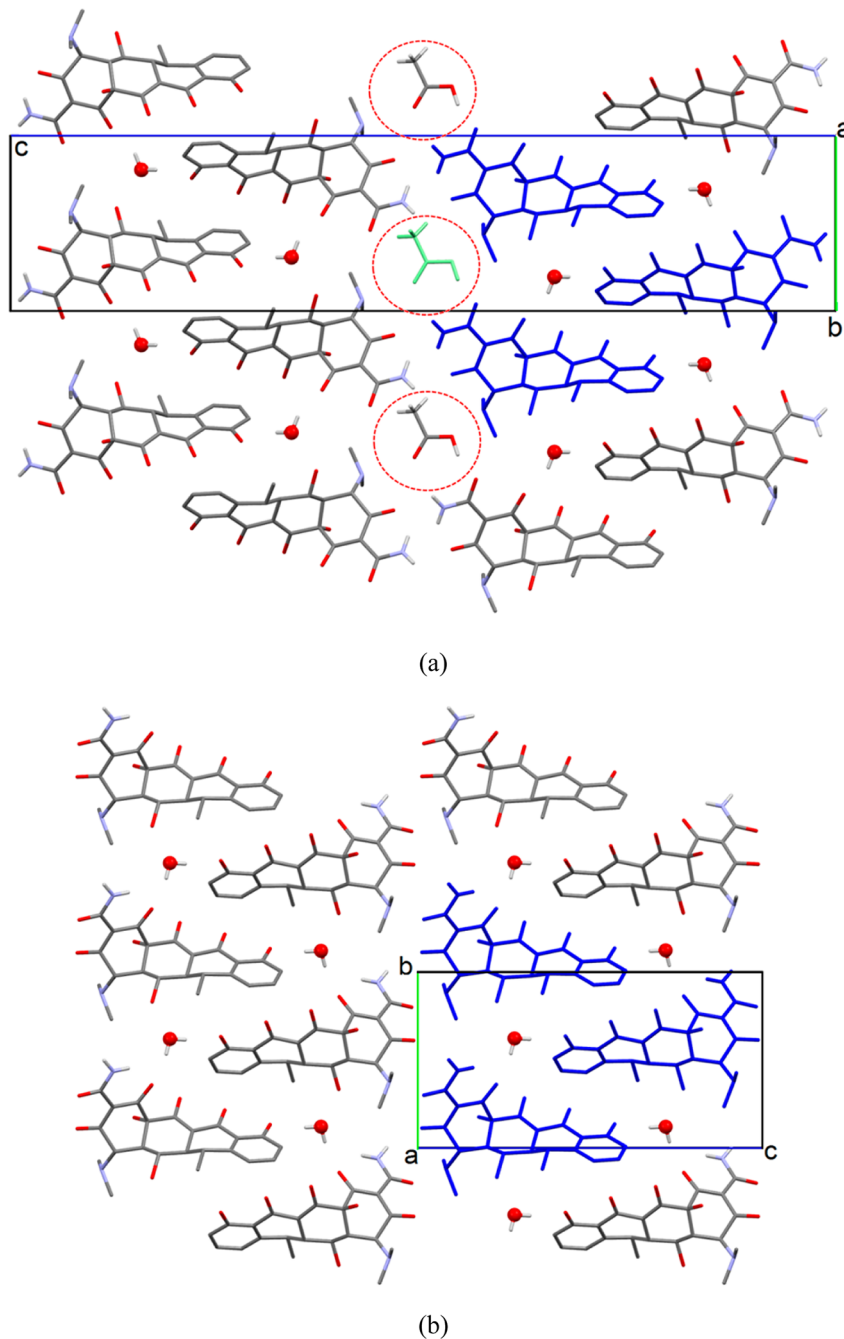


**Figure 7.** Packing views of DOX-HAc·2H<sub>2</sub>O (a) and DOX·H<sub>2</sub>O (b) onto plane bc. The DOX molecules in blue highlight the common synthon defined by the intermolecular HB. Acid acetic molecules layered between the chains are formed by the synthons along [010] (red dotted circles). Some hydrogens were omitted for clarity.

similar in the two crystal phases assembled with zwitterionic DOX molecules, emphasizing the fact that their O8 is not protonated. In addition, the position parameters of the acidic H9 hydrogen covalently bonded to the carboxyl O9 oxygen were first located using the difference Fourier map. H9 was freely refined and associated with common carboxyl C=O and C—O bond lengths of 1.310(3) Å and 1.217(3) Å, which were found here. This free refinement with HAc instead of carboxylate C—O<sup>-</sup> bonds has allowed us to assign neutrality to the carboxylic acid when crystallized with DOX.

**3.3. Intermolecular Hydrogen Bonding (HB) Patterns and Packing Features.** DOX and HAc give rise to a R<sub>2</sub><sup>(8)</sup> ring through their amide and carboxyl supramolecular

functionalities, respectively (Figure 6). The DOX-HAc pairs assembled through this motif are further packed along the [100] direction by means of the N1—H1a···O10 HB moiety. In addition, one water molecule interacts with three DOX molecules in DOX-HAc·2H<sub>2</sub>O, acting as an HB donor to the carbonyl O6 oxygen and hydroxyl O1 and as acceptor from the hydroxyl O4 (Figure 2). Interestingly, such an intermolecular array is also found in DOX·H<sub>2</sub>O even though O6 is a bifurcated HB acceptor in this known structure due to its engagement in the S<sub>1</sub><sup>(6)</sup> cycle (see another related paper<sup>8</sup>). Moreover, this supramolecular synthon results in a very similar packing of DOX-HAc·2H<sub>2</sub>O and DOX·H<sub>2</sub>O even though the presence of the acid acetic and the additional water in DOX-HAc·2H<sub>2</sub>O

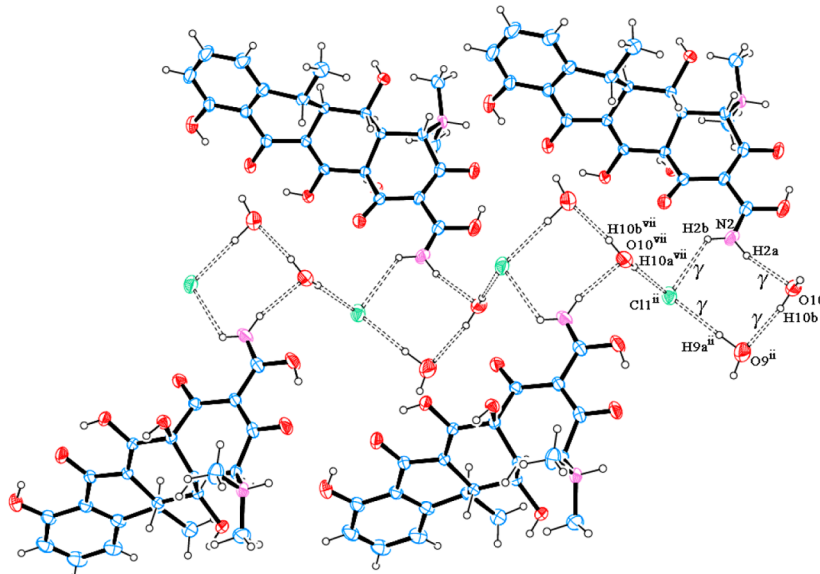


**Figure 8.** Intermolecular  $R_4^3(8)$  ring assembled with  $\gamma$ -labeled HB and their array along the [100] direction in DOX-HCl· $2H_2O$ . Symmetry transformations: (ii)  $(-x + 1, y + 0.5, -z + 1.5)$  and (vii)  $(x - 0.5, -y + 2.5, -z + 1)$ .

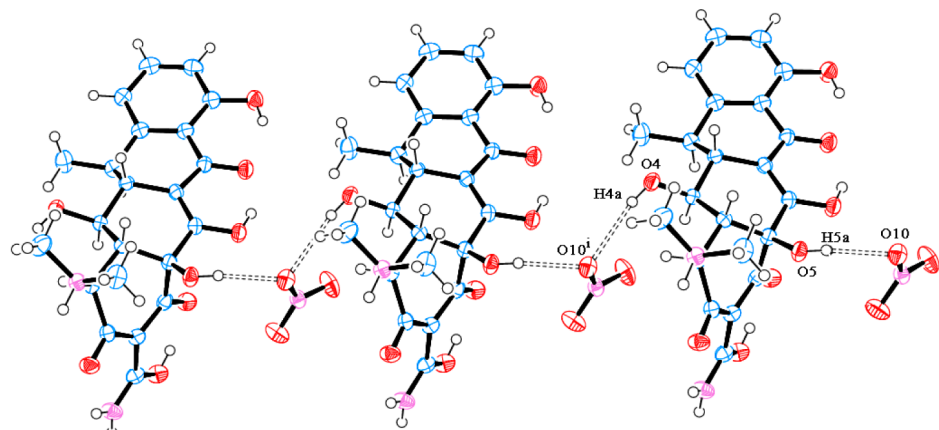


**Figure 9.** Intercalation between DOX- $HNO_3 \cdot 0.5H_2O$  T2 units by the crystallographically balanced nitrate counterion along the [010] direction. Symmetry transformation: (i)  $(x, y - 1, z)$ .

(Figure 7). Indeed, the acetic acid molecules appears to intercalate parallel to (002). However, the packing of DOX-HAc· $2H_2O$  and DOX- $H_2O$  also shows differences. While drug units do not interact directly in DOX-HAc· $2H_2O$ , there is an  $R_2^2(8)$  ring formed between two DOX molecules in the monohydrate form. The other water found in the solvent described here is responsible for cross-linking DOX molecules parallel to the  $a$ -axis by HB accepting from the hydroxyl OS oxygen. This hinders the assembly of the  $S_3^2(13)$  intramolecular pattern observed in DOX- $H_2O$  and results in a bifurcated HB donation to O6 and O8 (Figure 5).

In DOX-HCl· $2H_2O$ , two water molecules are intercalated between DOX and chloride, forming ionic pairs that are distributed along the [100] direction in infinite chains of units (Figure 4). Protonated N1 nitrogen also contributes to the stabilization of this supramolecular chain through the N1–H1a…O10 HB. This type of HB set can be generalized by either  $C_5^3(11)$  or  $R_6^4(13)$  motifs (Figure 4). The chains are cross-linked by two HBs with an amide  $NH_2$  functionality donating to both the water O10 oxygen and chloride. These N2–H2a…O10 and N2–H2b…Cl1 contacts assemble an  $R_4^3(8)$

motif together with O10–H10b…O9 and O9–H9…Cl1 HBs belonging to the  $C_5^3(11)$  backbone (Figure 8). In addition, there is only one HB directly linking the DOX molecules in the hydrochloride salt dihydrate structure. This O4–H4…O3 interaction occurs through hydroxyl groups from the  $2_1$ -screw axis symmetry-related drug molecules, connecting them along the [010] direction (Figure 3). The hydroxyl O4 oxygen also accepts a HB from water. Both contacts also act as cross-linkers between the  $C_5^3(11)$  supramolecular entities.

The asymmetric unit of DOX- $HNO_3 \cdot 0.5H_2O$  is present with two protonated DOX molecules named T1 and T2, two nitrate counterions (one of these is distributed over two positions) and one water molecule (Figure S3, Supporting Information). Each atom of the nitrate occupies only one site and intercalates with the T2 units along the [010] direction through its O10 acting as a bifurcated HB acceptor interacting with O4–H4 and O5–H5 (Figure 9). O11, another oxygen atom of this same nitrate unit, is also a bifurcated HB acceptor and interacts with the protonated N1–H1a moiety of T1 and O12–H12b of water (Figure S6, Supporting Information). The O12 oxygen from water is also a HB acceptor that interacts with the protonated

N1–H1a moiety of T2. This supramolecular pattern is responsible for intercalating T2 tautomers along the [100] direction through hydrogen-bonded nitrate and water molecules. T1 and T2 tautomers are intercalated along the [001] direction by a nitrate counterion (Figure S6, Supporting Information). Each atom of the other nitrate occupies two crystallographic sites. Three oxygen fractions (O13, O14, and O15) have major occupancy site factors (s. o. f.) of 0.599(8) that are HB acceptors from the O4–H4 hydroxyl group of T1 (O13), the N2–H2a moiety of T2 (O14), and O12–H12a of water (O15). Only the O14' and O15' oxygen fractions in the minor occupancy sites (s. o. f. of 0.401(8)) are HB acceptors from the same groups acting as HB donors to the major occupancy nitrate (Figure S7, Supporting Information). Although O15' is involved in a bifurcated HB with O4–H4 and O12–H12a moieties, the most favorable geometrical parameters for the interactions (donor–acceptor distances and D–H···A angles shown in Table 2) help to rationalize the s. o. f. values refined for the predominant nitrate fraction in the crystal lattice. Finally, a weak bifurcated HB in which the N2–H2a moiety of the amide is a donor to both hydroxyl O3 and O5 oxygens, connecting the T1 molecules along the *a* axis (Figure S6, Supporting Information).

**3.4. Powder X-ray Diffraction Analysis.** The calculated PXRD patterns for each crystal structure matched experimental patterns, although preferred orientation was observed. For instance, the preferred orientation was observed in  $2\theta$  equal to  $22.7^\circ$  ( $h k l = 2 \bar{1} 1$ ) for DOX·NO<sub>3</sub>·0.5H<sub>2</sub>O and in  $2\theta$  equal to  $19.7^\circ$  ( $h k l = 1 \bar{1} 5$ ) for DOX·HAc·2H<sub>2</sub>O (Figure S8, Supporting Information). Because neither pronounced broad humps from amorphous solid nor extra Bragg reflections from DOX crystalline phases other than that of the sample were observed in the experimental diffractograms, it was possible to conclude that DOX·NO<sub>3</sub>·0.5H<sub>2</sub>O, DOX·HAc·2H<sub>2</sub>O, and DOX·HCl·2H<sub>2</sub>O were the bulk of the crystal phases elucidated here.

**3.5. Thermal Analysis.** The DSC and TG curves of the crystal forms of DOX described in this study as well as the previously known DOX crystals are shown in Figures 10 and 11, respectively.

Although the MSDSs from several chemical manufacturers report a melting point for DOX·HYC, its TG curve shows a mass loss beginning at  $123^\circ\text{C}$  (DSC peak at  $170^\circ\text{C}$ ). This proves that the compound actually undergoes thermal decomposition (which corroborates the Merck Index<sup>28</sup> data, “*Chars without melting*”). This occurs even under an inert atmosphere in which a higher stability could be expected in comparison to air. Other experiments using lower heating rates were performed in order to try to establish a baseline between the first and second mass losses, but the curve profile remained the same and no thermally stable intermediates could be isolated or identified due to simultaneous and/or sequential decomposition reactions. According to the mass losses, these reactions are not strictly related to the release of solvent molecules or hydrochloric acid. This is very important data because it shows that the water and ethanol molecules in DOX·HYC confer such stability to the crystal lattice of the solid that, when the solvent molecules are finally released due to heating, the temperature is already high enough to cause the decomposition of the DOX molecule.

Regarding DOX·H<sub>2</sub>O, the first mass loss observed in the TG curve refers to the dehydration of the sample ( $T_i = 81^\circ\text{C}$ ;  $T_f = 127^\circ\text{C}$ ; DSC peak at  $158^\circ\text{C}$ ;  $\Delta m_{\text{TG}} = 4.0\%/\Delta m_{\text{calc.}} = 3.9\%$ ) following a baseline up to  $162^\circ\text{C}$ , when thermal decomposition

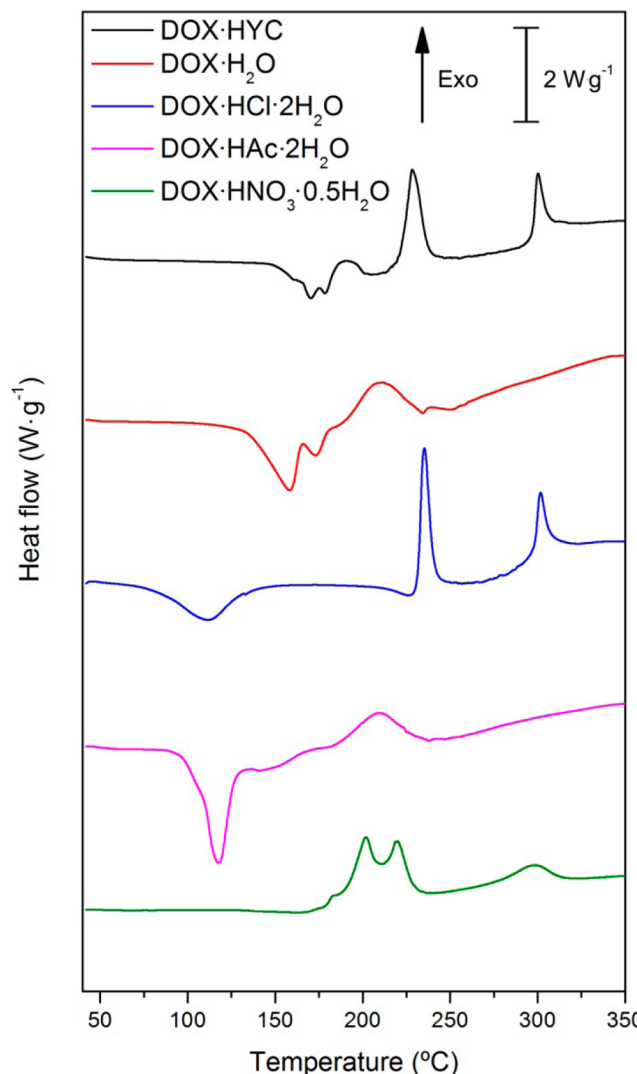


**Figure 10.** DSC curves of DOX·HYC, DOX·H<sub>2</sub>O, DOX·HCl·2H<sub>2</sub>O, DOX·HAc·2H<sub>2</sub>O, and DOX·HNO<sub>3</sub>·0.5H<sub>2</sub>O were measured in hermetic aluminum crucibles (sample and reference) at a heating rate of  $10^\circ\text{C min}^{-1}$  under a dynamic nitrogen atmosphere flowing at  $50\text{ mL min}^{-1}$ .

of the sample takes place (DSC peak at  $235^\circ\text{C}$ ). Visual inspection of the sample during heating indicated that the dehydration step did not lead to any change in the appearance of the material. Thus, we can confirm that the anhydrous DOX·H<sub>2</sub>O undergoes decomposition instead of melting. The anhydrous form of DOX·H<sub>2</sub>O could be produced by heating. However, the PXRD pattern obtained after  $130^\circ\text{C}$  (Figure S9, Supporting Information) shows that as soon as the solid is cooled and handled, it very rapidly takes water molecules from moist air and returns to the hydrated form. This precludes its use as an alternative crystal form of this API.

The TG curve of DOX·HCl·2H<sub>2</sub>O exhibits the loss of two water molecules in the first step ( $T_i = 40^\circ\text{C}$ ;  $T_f = 129^\circ\text{C}$ ; DSC peak at  $111^\circ\text{C}$ ;  $\Delta m_{\text{TG}} = 6.8\%/\Delta m_{\text{calc.}} = 7.0\%$ ). The anhydrous compound is stable up to  $183^\circ\text{C}$  when its thermal decomposition slowly begins. The same remark on anhydrous DOX applies here: DOX·HCl can be obtained by heating DOX·HCl·2H<sub>2</sub>O, but the anhydrous form takes water up so rapidly that it could not be isolated for adequate chemical characterization. The PXRD pattern obtained after heating at

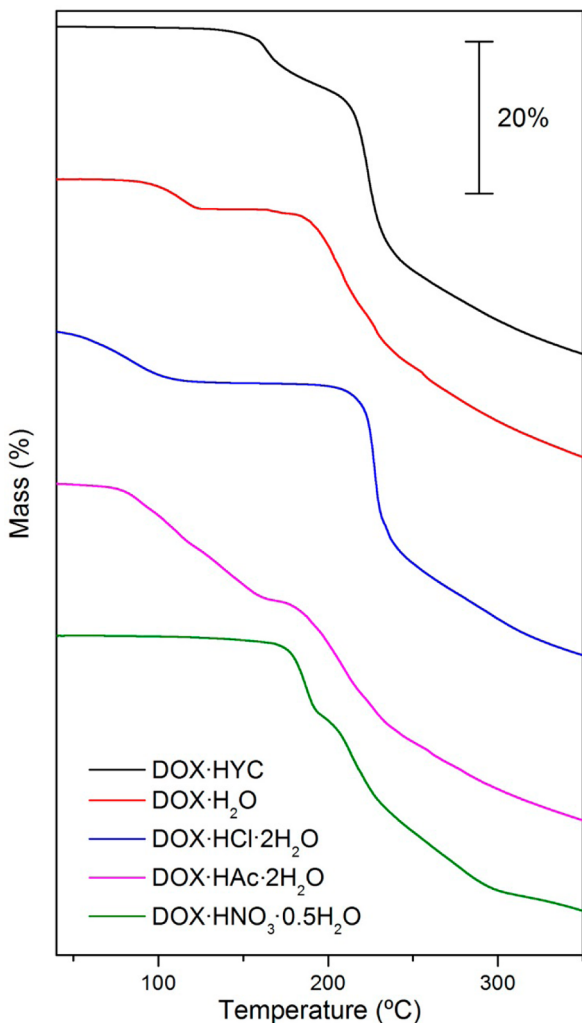


**Figure 11.** TG curves of DOX·HYC, DOX·H<sub>2</sub>O, DOX·HCl·2H<sub>2</sub>O, DOX·HAc·2H<sub>2</sub>O, and DOX·HNO<sub>3</sub>·0.5H<sub>2</sub>O obtained from sample masses of approximately 4 mg placed on open aluminum crucibles and heated at a rate of 10 °C min<sup>-1</sup> under a 50 mL min<sup>-1</sup> dynamic nitrogen atmosphere.

130 °C yielded DOX·HCl·2H<sub>2</sub>O (Figure S10, Supporting Information), confirming a fast hydration of the anhydrous DOX·HCl phase.

The characteristic smell of acetic acid noticed in DOX·HAc·2H<sub>2</sub>O corroborates the relatively weak interaction between this acid and the drug molecule. Its TG curve confirms this possibility. In fact, the first decomposition stage for DOX·HAc·2H<sub>2</sub>O ( $T_i = 73$  °C;  $T_f = 160$  °C; DSC peak at 118 °C;  $\Delta m_{TG} = 15.6\%/\Delta m_{calc.} = 17.8\%$ ) is due to the simultaneous release of acetic acid and both water molecules, and the real mass loss was smaller than expected because some water and acetic acid molecules were most likely carried by the purge gas before the heating ramp started. The compound begins to decompose at 176 °C, almost immediately after the loss of water and acetic acid.

Unlike the previously characterized forms, DOX·HNO<sub>3</sub>·0.5H<sub>2</sub>O loses water very slowly ( $T_i = 48$  °C;  $T_f = 138$  °C;  $\Delta m_{TG} = 0.5\%/\Delta m_{calc.} = 1.8\%$ ). Thus, no endothermic peak was observed in the DSC curve. The anhydrous form is stable up to 163 °C and then undergoes decomposition. The first peak in the DSC curve of DOX·HNO<sub>3</sub>·0.5H<sub>2</sub>O, in contrast with the

other crystal forms, is exothermic due to the oxidant nature of the nitrate ion. Considering the anhydrous forms of the studied DOX derivatives, the following thermal stability order could be established: DOX·HYC < DOX·H<sub>2</sub>O  $\cong$  DOX·HNO<sub>3</sub>·0.5H<sub>2</sub>O < DOX·HAc·2H<sub>2</sub>O < DOX·HCl·2H<sub>2</sub>O.

In general, when polymorphs of a same molecule (including API) are compared, the solid state phase with a lower MT and thus a higher lattice free energy is expected to have a higher equilibrium solubility and faster dissolution rate.<sup>29</sup> However, these predictions are confounded when multicomponent forms of a molecule are considered, as observed for DOX·H<sub>2</sub>O and DOX·HYC in the previous study.<sup>8</sup>

**3.6. Infrared Analysis.** The infrared spectra obtained for each studied doxycycline form are shown in Figure S11 (Supporting Information). Because the structural cores of all forms are essentially the same, there are no significant differences in their spectra. In addition, several bands present shoulders or are asymmetric due to the superimposition of groups with close vibrational frequencies of absorption and/or as consequence of hydrogen bonding. Table S3 (Supporting Information) exhibits the main bands and their assignments. The bands corresponding to crystallized water molecules appear at approximately 3550 cm<sup>-1</sup> ( $\nu_a$ H<sub>2</sub>O) and 1600 cm<sup>-1</sup> ( $\delta$ H<sub>2</sub>O). The last band is in the same region as the scissoring NH<sub>2</sub> in the amide ( $\delta$ NH<sub>2</sub>). The OH stretching of the alcohol, enol, and phenol groups gives rise to broad bands and shoulders between 3500 and 3350 cm<sup>-1</sup>. Their decrease in energy reflects the occurrence of inter- and intramolecular hydrogen bonds, as confirmed by the single crystal diffractometry data. The bands of the asymmetric stretching ( $\nu_a$ NH<sub>2</sub> amide) of the amide group are between 3320 and 3280 cm<sup>-1</sup>, followed by those of the  $\nu$ CH<sub>ring</sub> (~3050 cm<sup>-1</sup>),  $\nu_a$ CH<sub>3</sub> (~2950 cm<sup>-1</sup>), and  $\nu_s$ CH<sub>3</sub> (~2850 cm<sup>-1</sup>). The bands arising from carbonyl ( $\nu$ C=O) and aromatic C–C bonds ( $\nu$ CC<sub>ring</sub>) lie in the region from 1700 to 1650 cm<sup>-1</sup>. The intense electronic delocalization comprising several atoms next to the amide, ketone, and enol as well as the abundant amount of hydrogen bonds involving these groups broadens the  $\nu$ C=O bands (in all spectra, they are broad and asymmetric). Thus, the IR data could not be satisfactorily used to identify or differentiate keto-enol tautomers in this case. The  $\nu$ CC<sub>ring</sub> bands are at 1570 and 1450 cm<sup>-1</sup> region while the  $\nu_s$ CH<sub>3</sub> band appears approximately 1550 cm<sup>-1</sup> and  $\delta$ CH<sub>ring</sub> at 1290 and 1240 cm<sup>-1</sup>. Finally, the  $\nu$ C–O vibrations arise at approximately 1170 cm<sup>-1</sup>. The fingerprint region below ca. 1200 cm<sup>-1</sup> is almost identical for all DOX forms.

**3.7. Equilibrium Solubility.** The solubility and dissolution rates of DOX were exhaustively studied for the known forms DOX·HCl·2H<sub>2</sub>O, DOX·HYC, and DOX·H<sub>2</sub>O by Bogardus and Blackwood in the late 1970s.<sup>27</sup> Their main conclusions concerning DOX solubility are summarized as follows:

(i)  $pK_a = 3.09$  ( $\mu = 1$  and 25 °C) for protonation of DOX ( $\text{DOXH}^{+,\pm} \rightarrow \text{DOX}^\pm + \text{H}^+$ ).

(ii) The pH-solubility profile for DOX reached a maximum of 50 g L<sup>-1</sup> at  $\text{pH}_{max}$  2.16, which was a result of the simultaneous equilibrium between  $\text{DOXH}^{+,\pm}$  and  $\text{DOX}^\pm$  in water. DOX·HCl·2H<sub>2</sub>O and DOX·H<sub>2</sub>O forms are the respective solid phases in equilibrium with the solution below and above this  $\text{pH}_{max}$ . The DOX·H<sub>2</sub>O solubility increases until the  $\text{pH}_{max}$  is reached due to protonation of DOX in solution.

(iii) Added chloride ion strongly suppressed the solubility of DOX·HCl·2H<sub>2</sub>O form in water due to the common ion effect.

(iv) The solubility of DOX·H<sub>2</sub>O form was enhanced by nitrate and chloride ions compared to water, which was attributed to the zwitterionic nature of DOX in water.

(v) The stable crystalline DOX form in aqueous hydrochloric acid is DOX·HCl·2H<sub>2</sub>O, which was isolated from solutions prepared with DOX·HYC.

Taking these known features into account, the equilibrium solubility of the two new DOX forms, DOX·HNO<sub>3</sub>·0.5H<sub>2</sub>O and DOX·HAc·2H<sub>2</sub>O, was measured in water and solutions/buffers with pH ranging from 1 to 7.5 and compared to the known forms DOX·HCl·2H<sub>2</sub>O, DOX·HYC, and DOX·H<sub>2</sub>O, which were measured in the same conditions. The results are presented in Figure 12.

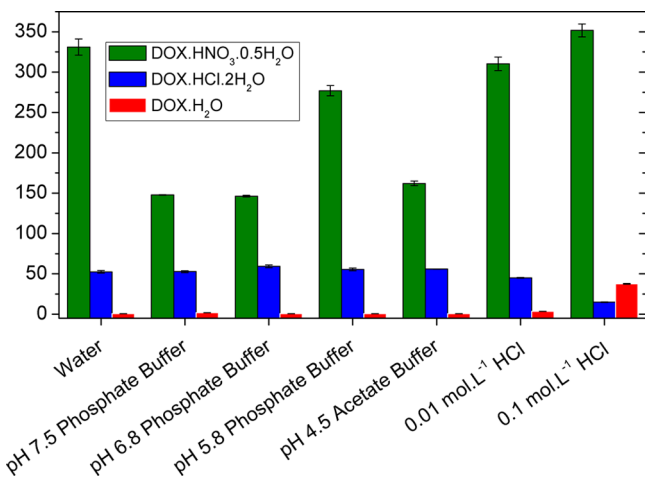


**Figure 12.** Values of equilibrium solubilities of DOX·H<sub>2</sub>O, DOX·HCl·2H<sub>2</sub>O, and DOX·HNO<sub>3</sub>·0.5H<sub>2</sub>O forms at 25 °C. Error bars represent standard deviations.

The solid material in equilibrium with the solutions used to determine the DOX equilibrium solubility were posteriorly dried and analyzed by PXRD. The results show that DOX·H<sub>2</sub>O, DOX·HCl·2H<sub>2</sub>O, and DOX·HNO<sub>3</sub>·0.5H<sub>2</sub>O remained in the solid phase in equilibrium in all dissolution media tested (Figures S12–S14, Supporting Information). On the other hand, DOX·HYC converted into DOX·HCl·2H<sub>2</sub>O as expected,<sup>27</sup> whereas DOX·HAc·2H<sub>2</sub>O converted into DOX·H<sub>2</sub>O in all dissolution media (Figures S15 and S16, Supporting Information).

The DOX·H<sub>2</sub>O equilibrium solubility shows the lowest values in water (0.64(1) g L<sup>-1</sup>, final pH ~5) and buffered media (0.61–1.99(2) g L<sup>-1</sup>, final pH values 4–7) compared to the other forms, which is expected in this pH range. The values observed are very similar to those found in the literature (0.75 g L<sup>-1</sup> in pH 4.0 buffer).<sup>27</sup> Also in agreement with previously published results, the equilibrium solubility of DOX·H<sub>2</sub>O in aqueous hydrochloric acid increases significantly to 3.48(5) g L<sup>-1</sup> in 0.01 mol L<sup>-1</sup> HCl (final pH ~2) and 37.7(5) g L<sup>-1</sup> in 0.1 mol L<sup>-1</sup> HCl (final pH ~2). These values are greater than those for DOX·HCl·2H<sub>2</sub>O (14.9(3) g L<sup>-1</sup>, final pH ~1) and comparable to those for DOX·HAc·2H<sub>2</sub>O (43(1) g L<sup>-1</sup>, final pH ~1) in the latter medium. The same final pH was observed for the two HCl solutions containing DOX·H<sub>2</sub>O. This is explained by the increased chloride concentration in HCl 0.1 mol L<sup>-1</sup>, which increases the DOX·H<sub>2</sub>O solubility due to the protonation of DOX in solution followed by an increase in pH. It is important to stress that no interconversion of DOX·H<sub>2</sub>O

to DOX·HCl·2H<sub>2</sub>O occurred during the experiment (Figure S12, Supporting Information) even in the hydrochloric acid media.

The equilibrium solubility values obtained for DOX·HYC could not be considered the actual values in any dissolution medium because the PXRD results (Figure S15, Supporting Information) show a conversion of the solid in equilibrium to the more thermodynamically stable form DOX·HCl·2H<sub>2</sub>O.<sup>27</sup> However, in all media the equilibrium concentrations of DOX prepared from DOX·HYC were significantly increased (~30% in water and buffered medium) compared to DOX·HCl·2H<sub>2</sub>O. It is well-known that DOX·HYC can be easily supersaturated by several-fold with respect to the solubility of DOX·HCl·2H<sub>2</sub>O due to the slow nucleation and/or crystal growth in the interconversion of aqueous DOX·HYC to DOX·HCl·2H<sub>2</sub>O.<sup>27</sup> The largest difference is observed by comparing the equilibrium solubility of DOX·HYC (43(1) g L<sup>-1</sup>, final pH ~1) and DOX·HCl·2H<sub>2</sub>O (14.9(3) g L<sup>-1</sup>, final pH ~1) in HCl 0.1 mol L<sup>-1</sup>, which is caused by the expected reduction in the equilibrium solubility of DOX·HCl·2H<sub>2</sub>O in the presence of the chloride ion.<sup>27</sup>

The equilibrium solubility values for DOX·HCl·2H<sub>2</sub>O were very similar in water and buffered medium. The mean value of 55(3) g L<sup>-1</sup> observed in these solutions agrees very well with that (50 g L<sup>-1</sup> in water pH 6.8–7.0) reported in the literature.<sup>27</sup> The acidic hydrolysis of DOX·HCl·2H<sub>2</sub>O goes down to final pH 2–3 even in buffered solutions. The common ion effect is responsible for the lower equilibrium solubility values observed for DOX·HCl·2H<sub>2</sub>O in HCl 0.01 (45.1(5) g L<sup>-1</sup>, final pH ~1) and 0.1 mol L<sup>-1</sup> (14.9(3) g L<sup>-1</sup>, final pH ~1).

DOX·HNO<sub>3</sub>·0.5H<sub>2</sub>O shows equilibrium solubility 2- to 3-fold greater than the other studied DOX forms, e.g., 331(10) g/L (final pH ~3), which is a remarkable feature of this work. The highest DOX·HNO<sub>3</sub>·0.5H<sub>2</sub>O solubility confirms the expected high solubility of nitrates, which is a consequence of the low hydration enthalpy and relatively high entropy of nitrate ion in water.<sup>30</sup>

Finally, in order to account for the DOX·HAc·2H<sub>2</sub>O equilibrium solubility, it is important to first emphasize its interconversion to DOX·H<sub>2</sub>O during the dissolution experiments, which was confirmed by PXRD (Figure S16, Supporting Information). Indeed, the interconversion of DOX·HAc·2H<sub>2</sub>O to DOX·H<sub>2</sub>O instead of DOX·HCl·2H<sub>2</sub>O in HCl 0.01 and 0.1 mol L<sup>-1</sup> was an unexpected result due to the presence of chloride in low pH that would favor the formation of DOX·HCl·2H<sub>2</sub>O. A reasonable explanation is that a conversion via solid state due to the layered character of DOX·HCl·2H<sub>2</sub>O made it easy to release acetic acid followed by the rearrangement of the strong supramolecular synthon shown in Figures 2 and 7.

Now considering the equilibrium solubility of solutions prepared with DOX·HAc·2H<sub>2</sub>O, the solution is supersaturated in water (39(2) g L<sup>-1</sup>, final pH ~3) by 65-fold with respect to the solubility of DOX·H<sub>2</sub>O (0.63(1) g L<sup>-1</sup>, final pH ~5). Similar increases were found for the buffered media. Therefore, as in DOX·HYC, the dissolution process appears to be faster than the interconversion to other crystal forms. Moreover, the dissolution of DOX·HAc·2H<sub>2</sub>O abruptly increased to ~140 g L<sup>-1</sup> in both hydrochloride solutions. In these two electrolyte solutions, DOX·HAc·2H<sub>2</sub>O is less soluble (by about half) than DOX·HNO<sub>3</sub>·0.5H<sub>2</sub>O.

**3.8. Forced Degradation Studies.** Table 3 shows that the new DOX forms (DOX·HAc·2H<sub>2</sub>O and DOX·HNO<sub>3</sub>·0.5H<sub>2</sub>O)

**Table 3. Percentage of DOX Forms after Forced Degradation Studies**

	DOX·H <sub>2</sub> O	DOX·HYC	DOX·HCl·2H <sub>2</sub> O	DOX·HNO <sub>3</sub> ·0.5H <sub>2</sub> O	DOX·HAc·2H <sub>2</sub> O
oxidation	38.8%	16.4%	41.4%	35.8%	39.4%
acid	96.3%	98.8%	100.5%	98.6%	99.9%
alkali	4.6%	10.1%	10.3%	10.6%	15.0%
neutral	96.5%	100.3%	99.8%	99.8%	96.9%
photostability	97.8%	103.9%	101.4%	100.7%	99.2%

were more stable than the commercial DOX·HYC against oxidation. The new forms were also more stable than commercial DOX·H<sub>2</sub>O against acid and basic hydrolysis as well as light exposure according to photodegradation studies. The PXRD patterns of the samples measured after the photostability study indicated no apparent phase transition (Figures S17, Supporting Information).

**3.9. Dissolution Profiles.** Dissolution profiles of the analyzed capsules are presented in Figure 13. The results are

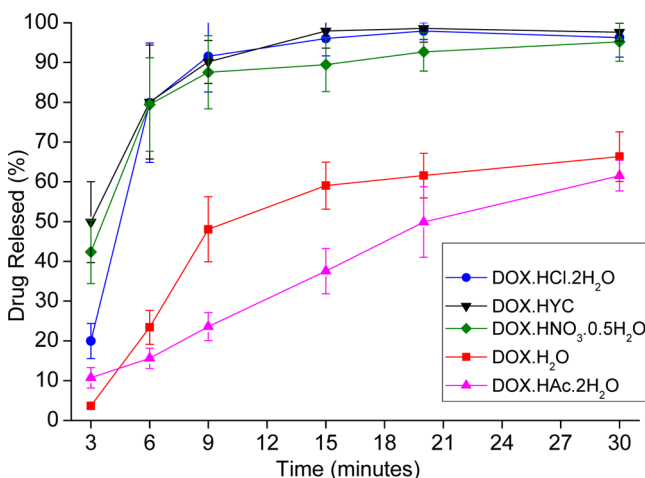


**Figure 13.** Dissolution profiles of tablets containing DOX forms. Error bars represent standard deviations.

expressed as percentage drug release versus time (min). A comparison study of the DOX forms in capsules was carried out using the similarity (F2) factor (Table 4). It was observed that DOX·HCl·2H<sub>2</sub>O and DOX·HNO<sub>3</sub>·0.5H<sub>2</sub>O have similar dissolution profiles (F2 > 50) to each other and to commercial

**Table 4. Similarity Factors Obtained from Comparison of the Dissolution Profiles between Pairs of DOX Forms in Capsules**

dissolutions profiles of capsules of DOX form evaluated	similarity factor (F2)
DOX·H <sub>2</sub> O vs DOX·HYC	18.4
DOX·H <sub>2</sub> O vs DOX·HCl·2H <sub>2</sub> O	20.7
DOX·H <sub>2</sub> O vs DOX·HAc·2H <sub>2</sub> O	41.3
DOX·H <sub>2</sub> O vs DOX·HNO <sub>3</sub> ·0.5H <sub>2</sub> O	20.9
DOX·HYC vs DOX·HCl·2H <sub>2</sub> O	79.0
DOX·HYC vs DOX·HAc·2H <sub>2</sub> O	12.8
DOX·HYC vs DOX·HNO <sub>3</sub> ·0.5H <sub>2</sub> O	63.0
DOX·HCl·2H <sub>2</sub> O vs DOX·HAc·2H <sub>2</sub> O	14.5
DOX·HCl·2H <sub>2</sub> O vs DOX·HNO <sub>3</sub> ·0.5H <sub>2</sub> O	50.2
DOX·HNO <sub>3</sub> ·0.5H <sub>2</sub> O vs DOX·HAc·2H <sub>2</sub> O	15.2

DOX·HYC. This result shows that we can expect the same therapeutic effect among these compounds and that they could be interchangeable. Thus, we include here the possibility of commercialization of nitrate doxycycline due to increasing medical interest in this oxyanion of nitrogen.<sup>31</sup> Moreover, the maximum recommended daily dosage of doxycycline is 200 mg divided into two doses per day; there are 24.4 mg of nitrate in this dosage. This is an amount that is in accordance with the values of acceptable daily intake (ADI) of nitrate established by The World Health Organization of up to 3.7 mg kg<sup>-1</sup> of body weight.<sup>32</sup> Considering that doxycycline is an antibiotic indicated for use in patients over eight years of age (25 kg approximate body mass), DOX·HNO<sub>3</sub>·0.5H<sub>2</sub>O could be responsible for only 26.4% of the acceptable daily intake of nitrate.

#### 4. CONCLUSION

Two novel crystal forms of DOX were prepared in this study. These were a hydronitrate salt hemihydrate and an acetic acid solvate dihydrate. Their crystal structures were inspected in full detail and compared to the structures of known DOX crystal forms. These included the hydrochloride salt dihydrate, which was also confirmed here, and its monohydrate and hydinate variants. Intramolecular rings assembled through RAHB were observed in both fused keto-enol moieties of all structures, but with different resonance assistance levels clearly denoted by planarity descriptors. Hydrated hydrochloride and hydronitrate salts have a further RAHB generated by the protonated amide carbonyl oxygen and the enolate oxygen. These forms have a net positive charge on both drug molecules and hydinate. Furthermore, nitrate salt hemihydrate is present with two tautomers (T1 and T2) and two amide moiety conformations, which are also observed in the hydinate form. Hydrochloride salt dihydrate has only one T1-like tautomer and therefore only one amide conformation similar to that of T1 tautomer in nitrate salt hemihydrate and hydinate. Similar to monohydrate form, acetic acid solvate dihydrate crystallizes as a zwitterion. Unlike all salts, the amide carbonyl oxygen of this crystal is not protonated. For the acetic acid solvate dihydrate form, a T1-like keto-enolate tautomer is present that exhibits an amide conformation related to that of T2. No RAHB occurs through the amide group of this crystal form even though this moiety is engaged in a S<sub>i</sub><sup>1</sup>(6) ring. In fact, this motif is present in all structures but without resonance assistance.

Interesting supramolecular patterns were identified. For instance, ionic pairs made up of DOX and chloride units are arranged along the [100] direction into C<sub>s</sub><sup>3</sup>(11) chains through intercalation of two water molecules between DOX and chloride in the hydrochloride salt dihydrate. The T1 and T2 tautomers are intercalated along the [001] direction by a crystallographically non-disordered nitrate counterion in the nitrate salt hemihydrate. In T2, one nitrate counterion occupies two crystallographic positions whose refined s.o. factors were rationalized by HB geometries. As a dihydrate in acetic acid solvent, DOX assembles with HAc into R<sub>2</sub><sup>2</sup>(8) hydrogen-bonded pairs, which are packed along the [100] direction into infinite one-dimensional chains.

The equilibrium solubility order in water and in all buffer solutions is invariantly as follows: DOX·HNO<sub>3</sub>·0.5H<sub>2</sub>O ≫ DOX·HYC (commercial form, converted into DOX·HCl·2H<sub>2</sub>O) > DOX·HCl·2H<sub>2</sub>O > DOX·HAc·2H<sub>2</sub>O (converted into DOX·H<sub>2</sub>O) ≫ DOX·H<sub>2</sub>O (commercial form). In addition to being the most soluble form, DOX·HNO<sub>3</sub>·0.5H<sub>2</sub>O is also as stable as both commercial forms and has similar dissolution

profiles when compared to DOX-HYC. Therefore, DOX·HNO<sub>3</sub>·0.5H<sub>2</sub>O may be a potential API for incorporation into commercial solid dosage forms of DOX.

## ■ ASSOCIATED CONTENT

### § Supporting Information

Tables S1–S3 and Figures S1–S17. This material is available free of charge via the Internet at <http://pubs.acs.org>. Crystallographic data have been deposited to the Cambridge Crystallography Data Centre with deposition numbers CCDC 974379, 974380, and 974381 for DOX·HAc·2H<sub>2</sub>O, DOX·HNO<sub>3</sub>·0.5H<sub>2</sub>O, and DOX·HCl·2H<sub>2</sub>O, respectively.

## ■ AUTHOR INFORMATION

### Corresponding Authors

\*E-mail: doriguetto@unifal-mg.edu.br. Phone: +55 35 3299 1261. Fax: +55 35 3299 1261.

\*E-mail: felipeterramartins@gmail.com.

### Notes

The authors declare no competing financial interest.

## ■ ACKNOWLEDGMENTS

We thank FAPEMIG (APQ-02600-12 and PPM-00524-12), FINEP (ref. 134/08 and 0336/09), CNPq (308354/2012-5 and 476870/2011-9), and CAPES (PNPD-2007 and PNPD-2011) for their financial support. We also thank CAPES, PIBICT-FAPEMIG and CNPq for research fellowships (AOL, DMS, IMLR, FTM, and ACD). We express sincere thanks to LabCri-UFMG for the X-ray facilities; Laboratório de Tecnologia Farmacêutica-UNIFAL-MG for the HPLC analysis; and Laboratório de Caracterização de Fármacos-UNIFAL-MG for the thermal analysis.

## ■ REFERENCES

- (1) Mokabberi, R.; Haftbaradaran, A.; Ravakhah, K. Doxycycline vs. levofloxacin in the treatment of community-acquired pneumonia. *J. Clin. Pharm. Ther.* **2010**, *35*, 195.
- (2) Elston, D. M. Tick bites and skin rashes. *Curr. Opin. Infect. Dis.* **2010**, *23*, 132.
- (3) Ziegler, T.; Winkler, C.; Wege, K.; Schmeichel, H. Doxycycline—the forgotten antibiotic. *Med. Klin.* **2000**, *95*, 629.
- (4) Griffin, M. O.; Fricovsky, E.; Ceballos, G.; Villarreal, F. Tetracyclines: a pleiotropic family of compounds with promising therapeutic properties. Review of the literature. *Am. J. Physiol. Cell. Physiol.* **2010**, *299*, C539.
- (5) Pallares, R.; Fenoll, A.; Liñares, J. The epidemiology of antibiotic resistance in *Streptococcus pneumoniae* and the clinical relevance of resistance to cephalosporins, macrolides and quinolones. *Int. J. Antimicrob. Agents* **2003**, *22*, S15.
- (6) Cunha, B. A. New uses for older antibiotics: nitrofurantoin, amikacin, colistin, polymyxin B, doxycycline, and minocycline revisited. *Med. Clin. N. Am.* **2006**, *90*, 1089.
- (7) Stezowski, J. J. Chemical-structural properties of tetracycline antibiotics. 4. Ring A tautomerism involving the protonated amide substituent as observed in the crystal structure of  $\alpha$ -6-deoxyoxytetracycline hydrochloride. *J. Am. Chem. Soc.* **1977**, *99*, 1122.
- (8) Legendre, A. O.; Silva, L. R. R.; Silva, D. M.; Rosa, I. M. L.; Azarias, L. C.; Abreu, P. J.; Araújo, M. B.; Neves, P. P.; Torres, C.; Martins, F. T.; Doriguetto, A. C. Solid state chemistry of the antibiotic doxycycline: structure of the neutral monohydrate and insights into its poor water solubility. *CrystEngComm* **2012**, *14*, 2532.
- (9) Heinemann, F. W.; Leybold, C. F.; Roman, C. R.; Schmitt, M. O.; Schneider, S. X-ray crystallography of tetracycline, doxycycline and sencycline. *J. Chem. Crystallogr.* **2013**, *43*, 213.
- (10) Bordner, J. Structure of  $\beta$ -6-deoxyoxytetracycline hydrochloride. *Acta Crystallogr.* **1979**, *B35*, 219.
- (11) (a) Brittain, H. G. Book review of polymorphism in the pharmaceutical industry. *Cryst. Growth Des.* **2008**, *8*, 2588. (b) Aitipamula, S.; Chow, P. S.; Tan, R. B. H. Polymorphs and solvates of a cocrystal involving an analgesic drug, etenazamide, and 3,5-dinitrobenzoic acid. *Cryst. Growth Des.* **2010**, *10*, 2229. (c) Babu, N. J.; Nangia, A. Solubility advantage of amorphous drugs and pharmaceutical cocrystals. *Cryst. Growth Des.* **2011**, *11*, 2662. (d) Martin, F. A.; Pop, M. M.; Borodi, G.; Filip, X.; Kacsó, I. Ketoconazole salt and co-crystals with enhanced aqueous solubility. *Cryst. Growth Des.* **2013**, *13*, 4295.
- (12) *CrysAlis Pro*, v 1.7; Oxford Diffraction Ltd, Abingdon, England, 2006.
- (13) Sheldrick, G. M. A short history of SHELX. *Acta Crystallogr.* **2008**, *A64*, 112.
- (14) Cianci, M.; Helliwell, J. R.; Helliwell, M.; Kaucic, V.; Logar, N. Z.; Mali, G.; Tusar, N. N. Anomalous scattering in structural chemistry and biology. *Crystallogr. Rev.* **2005**, *11*, 245.
- (15) Farrugia, L. J. WinGX suite for small-molecule single-crystal crystallography. *J. Appl. Crystallogr.* **1999**, *32*, 837.
- (16) Macrae, C. F.; Bruno, I. J.; Chisholm, J. A.; Edgington, P. R.; McCabe, P.; Pidcock, E.; Rodriguez-Monge, L.; Taylor, R.; Streck, J.; Wood, P. A. Mercury CSD 2.0 - new features for the visualization and investigation of crystal structures. *J. Appl. Crystallogr.* **2008**, *41*, 466.
- (17) Farrugia, L. J. ORTEP-3 for Windows - a version of ORTEP-III with a Graphical User Interface (GUI). *J. Appl. Crystallogr.* **1997**, *30*, 565.
- (18) Skúlason, S.; Ingólfsson, E.; Kristmundsdóttir, T. Development of a simple HPLC method for separation of doxycycline and its degradation products. *J. Pharm. Biomed. Anal.* **2003**, *33*, 667.
- (19) International Conference on Harmonization (ICH). Technical Requirements for the Registration of Pharmaceuticals for Human Use. Stability Testing of New Drugs Substance and Products Q1A(R2), 2003.
- (20) Glomme, A.; März, J.; Dressman, J. B. Comparison of a miniaturized shake-flask solubility method with automated potentiometric acid/base titrations and calculated solubilities. *J. Pharm. Sci.* **2005**, *94*, 1.
- (21) *Dissolution Testing of Immediate Release Solid Oral Dosage Forms; Guidance for Industry*; U.S. Department of Health and Human Services, Food and Drug Administration, Center for Drug Evaluation and Research (CDER); U.S. Government Printing Office: Washington, DC, 1997.
- (22) Santos, O. M. M.; Santos, A. L. A.; Pereira, G. R.; Bonfilio, R.; Araújo, M. B. A dissolution test for finasteride in immediate-release capsules. *Dissolution Technologies* **2013**, *20*, 25.
- (23) (a) Bernstein, J.; Davis, R. E.; Shimoni, L.; Chang, N. L. Patterns in hydrogen bonding: functionality and graph set analysis in crystals. *Angew. Chem., Int. Ed. Engl.* **1995**, *34*, 1555. (b) Etter, M. C.; Reutzel, S. M. Hydrogen-bond directed cocrystallization and molecular recognition properties of acyclic imides. *J. Am. Chem. Soc.* **1991**, *113*, 2586.
- (24) Allen, F. H. The Cambridge Structural Database: a quarter of a million crystal structures and rising. *Acta Crystallogr.* **2002**, *B58*, 380–388.
- (25) Bhogala, B. R.; Basavojju, S.; Nangia, A. Tape and layer structures in cocrystals of some di- and tricarboxylic acids with 4,4'-bipyridines and isonicotinamide. From binary to ternary cocrystals. *CrystEngComm* **2005**, *7*, 551.
- (26) Cruz-Cabeza, A. Acid-base crystalline complexes and pK<sub>a</sub> rule. *CrystEngComm* **2012**, *14*, 6362.
- (27) (a) Borgadus, J. B.; Blackwood, R. B., Jr. Dissolution rates of doxycycline free base and hydrochloride salts. *J. Pharm. Sci.* **1979**, *68*, 1183. (b) Borgadus, J. B.; Blackwood, R. B., Jr. Solubility of doxycycline in aqueous solution. *J. Pharm. Sci.* **1979**, *68*, 188.
- (28) Windholz, M. Ed.; *The Merck index: Encyclopedia of chemicals, drugs and biologicals*, 10th ed., Merck & Co., Inc.: New Jersey, 1983, Entry# 3436. pp 2067.

- (29) Khankari, R. K.; Grant, D. J. K. Pharmaceutical hydrates. *Thermochim. Acta* **1995**, *248*, 61.
- (30) Silva, L. A.; Martins, C. R.; de Andrade, J. B. Por que todos os nitratos são solúveis? *Quim. Nova* **2004**, *27*, 1016
- (31) Butler, A. R.; Feelisch, M. Therapeutic uses of inorganic nitrite and nitrate: from the past to the future. *Circulation* **2008**, *117*, 2151.
- (32) Hambridge, T. Intake assessment: WHO Food Additives Series: Nitrate and Nitrite. Available in <http://www.inchem.org/documents/jecfa/jecmono/v50je07.htm#3.2>; Accessed on May 31, 2014.